

# Branching Flows: Discrete, Continuous, and Manifold Flow Matching with Splits and Deletions

Lukas Billera<sup>\*1</sup>, Hedwig Nora Nordlinder<sup>\*1</sup>, Jack Collier Ryder<sup>1</sup>, Anton Oresten<sup>1</sup>, Aron Stålmårck<sup>1</sup>, Theodor Moseetti Björk<sup>1</sup>, Ben Murrell<sup>1</sup>

<sup>1</sup>Department of Microbiology, Tumor and Cell Biology, Karolinska Institutet, <sup>\*</sup>Contributed equally

Diffusion and flow matching approaches to generative modeling have shown promise in domains where the state space is continuous, such as image generation or protein folding & design, and discrete, exemplified by diffusion large language models. They offer a natural fit when the number of elements in a state is fixed in advance (e.g. images), but require *ad hoc* solutions when, for example, the length of a response from a large language model, or the number of amino acids in a protein chain is not known *a priori*.

Here we propose Branching Flows, a generative modeling framework that, like diffusion and flow matching approaches, transports a simple distribution to the data distribution. But in Branching Flows, the elements in the state evolve over a forest of binary trees, branching and dying stochastically with rates that are learned by the model. This allows the model to control, during generation, the number of elements in the sequence. We also show that Branching Flows can compose with any flow matching base process on discrete sets, continuous Euclidean spaces, smooth manifolds, and ‘multimodal’ product spaces that mix these components. We demonstrate this in three domains: small molecule generation (multimodal), antibody sequence generation (discrete), and protein backbone generation (multimodal), and show that Branching Flows is a capable distribution learner with a stable learning objective, and that it enables new capabilities.

**Date:** November 12, 2025

**Correspondence:** benjamin.murrell@ki.se

## 1 Introduction

For many applications that involve generating a sequence of elements, it isn’t possible to know the required number of elements in advance. For sequences of discrete tokens this is relatively well addressed by left-to-right autoregressive (AR) sequence models which can control the output length by sampling stop tokens. Diffusion and flow matching methods move beyond left-to-right AR structure, but sacrifice the ability to naturally handle variable-length outputs. Edit Flows, which models variable-length discrete sequences via insertions and deletions, was recently developed (Havasi et al., 2025) and expanded (Nguyen et al., 2025) to address this.

However for variable-length sequences over continuous spaces there are far fewer options. Continuous autoregressive models are possible (Billera et al., 2024). But in the continuous domain there are practical limitations specifically related to their autoregressive nature. Diffusion and flow models excel for structured grids and fixed-length sequences, but do not naturally handle variable-length outputs. Limited attempts to develop variable-length diffusion models exist (Campbell et al., 2023), but these rely on an approximation related to the addition of new elements, and it is unclear how they scale to more complex spaces than the ones upon which they were demonstrated.

One challenge not naturally addressed by fixed-length diffusion/flow models nor AR models (especially in the continuous state context) is what we call the ‘unknown-length infix sampling’ problem, where a segment of unknown length must be inserted into a sequence, conditioned on *a priori* known flanking regions. Even outside of this context, there is a ‘soft’ version of this problem that arises for fixed-length diffusion/flow models, where flanking regions happen to resolve early during an inference trajectory, and the model cannot

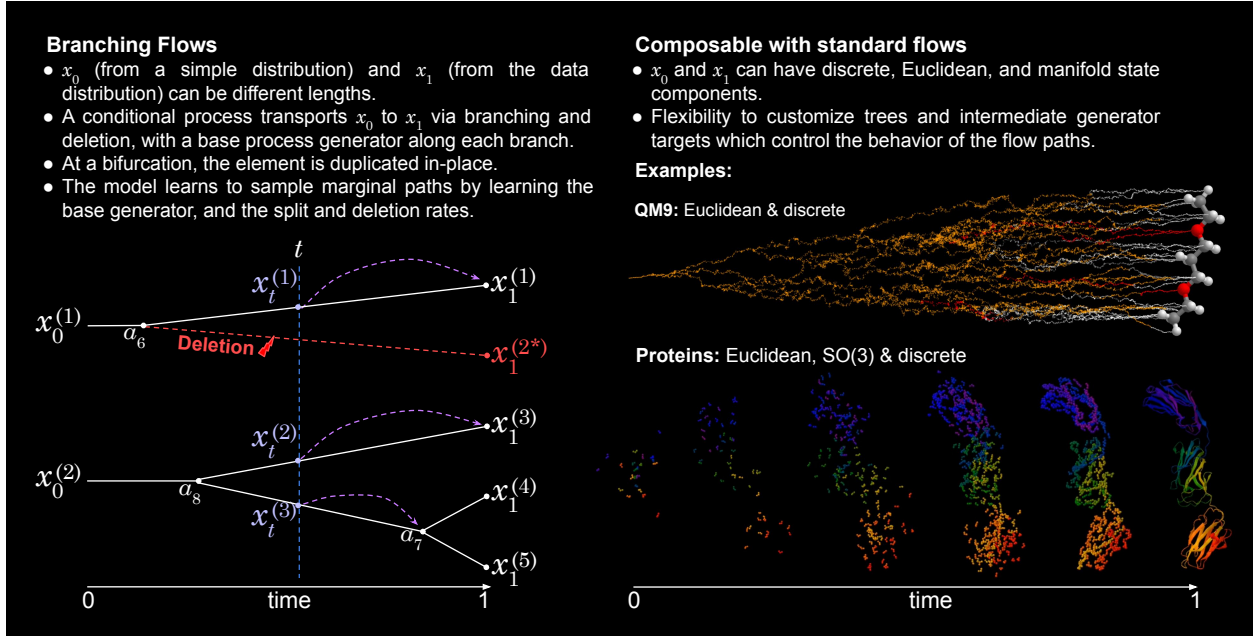


Figure 1: **Graphical Abstract.**

control the number of elements spanning them.

Here we present Branching Flows, which is a framework for generative modeling over variable-length sequences, where the elements can be continuous, manifold-valued, discrete, or combinations of these. This is formulated in Generator Matching (Holderrieth et al., 2024), where a conditional process transports samples from a simple distribution to samples from the data distribution. The generator of this conditional process is learned, in expectation, yielding a generator whose marginals match those of the conditional process. Branching Flows augments a base Markov generator on an element space with a branching and deletion process. A forest of trees that represents the branching structure is used to couple a sample from a simple distribution (with elements at the roots) with the data distribution (elements at the leaves). Much like the processes used in molecular evolution and phylogenetics (Felsenstein, 1981), the elements evolve independently along each branch but duplicate and decouple at bifurcations in the tree. We show how to use this construction, composed with optional deletions, to train a generative model with naturally hierarchical stochastic paths over sequences of varying length.

We demonstrate Branching Flows on small molecules, antibody sequences, as well as on protein structure generation, which is a real-world multimodal application involving Euclidean, manifold, and discrete states. Finally, we provide a flexible implementation that makes it simple to compose base processes into Branching Flows.

## 2 Preliminaries

### 2.1 Generator Matching

Following Generator Matching (Holderrieth et al., 2024; Lipman et al., 2024), for  $t \in [0, 1]$ , we seek a probability path  $p_t$  that interpolates between two fixed marginals  $p$  and  $q$ , where  $p$  is typically a distribution that is easy to sample from, and  $q$  is the data distribution. This goes via a conditional-path construction: Conditional on an auxiliary variable  $z \in \mathcal{Z}$  with marginal distribution  $p_Z$  and a family of conditional probability measures  $p_{t|Z}(dx | z)$ . The corresponding marginal path can be described by hierarchical sampling

$$Z \sim p_Z, \quad X_t | (Z = z) \sim p_{t|Z}(dx | z) \Rightarrow X_t \sim p_t(dx).$$

Choose the conditional family so that the boundary constraints  $p_0 = p$  and  $p_1 = q$  hold after marginalization. This is typically done by sampling an  $X_0 \sim p$  and an  $X_1 \sim q$  and having the process start at  $X_0$  and end at  $X_1$ .

The goal is then to parameterize a generator  $\mathcal{L}_t$  by a neural network  $\mathcal{L}_t^\theta$  and train it to generate the marginal path  $p_t$ . This is done by first drawing samples from the conditional path  $X_t \sim p_{t|Z}(dx | z)$ , and then training  $\mathcal{L}_t^\theta$  against the generators of the conditional paths  $\mathcal{L}_t^z$ . Taking gradient steps under a Bregman divergence loss encourages  $\mathcal{L}_t^\theta$  to learn the expectation of the conditional generator which, via a gradient identity, also trains it to generate the marginal path  $p_t$ .

## 2.2 Augmented Generator Matching and Auxiliary Generator Matching

We wish to train a model to sample from a target random variable  $X_1 \sim q(dx)$ . By ‘*Augmented Generator Matching*’ we mean: augment our process with  $G_t$  (with instances denoted by  $g_t$ ) for each  $t \in [0, 1]$ , yielding joint training samples  $(X_1, G_1) \sim p_1(dg|x_1)q(dx)$ . Throughout the generative process, the augmentation  $G_t$  evolves with  $X_t$ . We train a model to emit a generator to transport  $(X_0, G_0)$  to  $(X_1, G_1)$ , and discard  $G_1$  to recover samples from the marginal distribution  $q(dx)$ .

Additionally, one can use the augmented conditional paths, but train a model that marginalizes over  $G_t$ , learning a generator on  $X_t$  that generates samples from the data distribution  $q(dx)$  (this was shown in Edit Flows (Havasi et al., 2025) for the discrete case, but see Appendix D.1 for our setting). We will refer to this as ‘*Auxiliary Generator Matching*’.

## 2.3 Counting Flows and Deletion Flows

We first describe Counting Flows and Deletion Flows, which we will use to construct Branching Flows. See Appendix A for a full description of the infinitesimal generator of the process corresponding to having insertions and deletions with these rates, independently for each component.

### 2.3.1 Poisson Process ‘Counting Flow’

We first introduce ‘Counting Flows’: flow matching over a Poisson counting process that generates samples from the space of non-negative integer ‘counts’ via a conditional process that repeatedly increments by 1 to terminate at an observed count  $z_c$  by  $t = 1$ . This will later be repurposed for Branching Flows, but we present it here in isolation.

Let  $H_{\text{inc}}$  be some hazard distribution supported on  $[0, 1]$ , with its associated hazard rate

$$h_{\text{inc}}(t) = \frac{f_{H_{\text{inc}}}(t)}{1 - F_{H_{\text{inc}}}(t)}.$$

Note that since  $H_{\text{inc}}$  is supported on  $[0, 1]$ , we have that  $h_{\text{inc}}(t) \rightarrow \infty$  as  $t \nearrow 1$ .

Conditioned on an observed count  $z_c$  we construct a time-inhomogeneous CTMC on  $\{0, 1, \dots, z_c\}$  with rates

$$Q_t^{z_c}(x_t + 1|x_t) = (z_c - x_t)h_{\text{inc}}(t)I_{\{x_t < z_c\}},$$

and  $Q_t^{z_c}(x_t|x_t) = -Q_t(x_t + 1|x_t)$ , with  $Q_t^{z_c}(\cdot|x_t) = 0$  otherwise.

For any  $t$ , the increment rate is thus proportional to the number of increments remaining. Due to the exploding rate  $Q_t^{z_c}(x_t + 1|x_t)$  as  $t \nearrow 1$  when  $z_c > x_t$ , the process will almost surely terminate at  $z_c$ .

With  $R_t^{z_c} = z_c - x_t$  the remaining increments, and  $R_t^\theta$  a neural network’s prediction of the remaining increments, then

$$D_R(R_t^{z_c}, R_t^\theta) = R_t^\theta - R_t^{z_c} \log R_t^\theta$$

is a valid loss under an appropriately scaled time-dependent linear parametrization (Billera et al., 2025).

Under this process, the distribution of event times is  $H$  (see Appendix A.1.1) and for a given  $t, x_t, z_c$  we can efficiently sample the waiting time until the next increment event (see Appendix A.1.2) which we will need.

### 2.3.2 Deletion Flow Matching

We also describe a CTMC in the state space  $S = \{0, 1\}$ , where 0 is ‘present’ and 1 is ‘deleted’. Let  $H_{\text{del}}$  be a hazard distribution supported on  $[0, 1]$ , with its associated hazard rate

$$h_{\text{del}}(t) = \frac{f_{H_{\text{del}}}(t)}{1 - F_{H_{\text{del}}}(t)}$$

implying that  $h_{\text{del}}(t) \rightarrow \infty$  as  $t \nearrow 1$ . We represent the probability of a deletion by  $t = 1$  with  $Z_d \in \{0, 1\}$ . This is a conditioning variable which determines the conditional rate  $Q_t^{Z_d}(x|x_t)$ , defined by:

$$Q_t^{Z_d}(1|0) = Z_d h_{\text{del}}(t) \quad \text{and} \quad Q_t^{Z_d}(0|0) = -Q_t^{Z_d}(1|0),$$

along with  $Q_t^{Z_d}(\cdot|x_t) = 0$  for all other values of  $x_t$ . Conditional on  $Z_d = 1$ , corresponding to a deleted element, then  $Q_t^{Z_d}(x|x_t) \rightarrow \infty$  as  $t \nearrow 1$ . Hence, the process  $X_t|(Z_d = 1)$  will terminate in deletion at  $t = 1$  with probability 1. Let  $\rho_t^{z_d} = z_d$  and  $\rho_t^\theta$  be a neural network’s prediction of the probability of deletion by time  $t$ . Then

$$D_\rho(\rho_t^{z_d}, \rho_t^\theta) = -[z_d \log(\rho_t^\theta) + (1 - z_d) \log(1 - \rho_t^\theta)]$$

is a valid, per-term, conditional generator matching loss under an appropriately scaled time-dependent linear parameterization (Billera et al., 2025).

## 3 Branching Flows

In Generator Matching, conditioning on  $Z$  ensures that the conditional process terminates at a sample from the data distribution, and can be used to control the properties of the conditional paths. For example, ‘minibatch optimal transport’ flow matching (Tong et al., 2024) draws  $X_0$  and  $X_1$  jointly, attempting to minimize the distance between  $x_0, x_1$  pairs. With Branching Flows, we make *extensive* use of  $Z$ .

### 3.1 $Z$

At time  $t$  the state is an ordered list  $X_t = (X_t^{(1)}, \dots, X_t^{(L_t)})$  with variable length  $L_t$ , where each element  $X_t^{(i)}$  is a random variable on some space  $\mathcal{E}$ . An observation from the data distribution is  $x_1 = (x_1^{(1)}, \dots, x_1^{(\ell_1)}) \sim q$ , and a sample from the initial distribution is  $x_0 = (x_0^{(1)}, \dots, x_0^{(\ell_0)}) \sim p$ , where  $\ell_0$  does not necessarily equal  $\ell_1$ .

We augment our sequence at  $t = 1$  by inserting ‘to be deleted’ states  $\emptyset_1$ , each also in  $\mathcal{E}$ , into  $X_1$  yielding  $X_1^{+\emptyset}$ , such that  $X_1 = \psi_\emptyset(X_1^{+\emptyset})$  where  $\psi_\emptyset$  discards all ‘to be deleted’ states. We denote the length of  $X_1^{+\emptyset}$  as  $L_1^{+\emptyset}$ , and require that  $L_1^{+\emptyset} > L_0$  (condition 1).

We sample an ordered list of labeled binary rooted plane trees,  $\mathcal{T} = (\mathcal{T}_1, \dots, \mathcal{T}_{L_0})$ , where the root of each tree  $\mathcal{T}_i$  is associated with the element  $X_0^{(i)}$ . Each element of  $X_1^{+\emptyset}$  is associated with a single leaf of a single tree, such that the ordering of the leaves (since the trees are planar) matches the ordering of  $X_1^{+\emptyset}$ . All nodes in the tree are labeled ‘surviving’ except leaf nodes associated with ‘to be deleted’ states, which are labeled ‘deleted’.

The number of descendants of node  $n_i$  (including both surviving and deleted) is denoted  $w_i$ . We further decorate the tree with ‘anchors’  $\mathcal{A}$  such that each node has an anchor  $(A_1, \dots)$ , where  $A_i$  is a random variable on  $\mathcal{E}$ , requiring that the anchor of the surviving leaves equals the leaf-associated element of  $X_1^{+\emptyset}$  (condition 2), but the internal anchors  $\mathcal{A}^\mathcal{T}$  have no such constraint.

For Branching Flows,  $Z \sim p_Z$  is a tuple  $(X_1^{+\emptyset}, X_0, \mathcal{T}, \mathcal{A})$ , which is obtained by first sampling  $X_1 \sim q$ , and then sampling from  $p(x_1^{+\emptyset}, x_0, \mathcal{T}, \mathcal{A} | X_1 = x_1)$  according to a scheme that satisfies conditions 1 and 2 above, and that also admits a simple marginal  $p(x_0)$ . Note that, since  $\mathcal{T}$  carries labels for which leaves are deleted,  $X_1$  is recoverable from  $Z$ .

To sample  $Z$  in practice, to be able to ensure that conditions 1 and 2 are met, we factorize  $p(x_1^{+\emptyset}, x_0, \mathcal{T}, \mathcal{A} | x_1)p(x_1)$  as follows:

- **Data:**  $X_1 \sim q$

- **Initial:**  $X_0 \sim \mathcal{D}_0 | (X_1 = x_1)$
- **Data with deletions:**  $X_1^{+\phi} \sim \mathcal{D}_\phi | (X_1 = x_1, X_0 = x_0)$
- **Forest:**  $\mathcal{T} \sim \mathcal{D}_\mathcal{T} | (X_1^{+\phi} = x_1^{+\phi}, X_0 = x_0)$
- **Internal anchors:**  $\mathcal{A}^\mathcal{I} \sim \mathcal{D} | (X_1^{+\phi} = x_1^{+\phi}, X_0 = x_0, \mathcal{T})$  (note: the leaf anchors are already determined by  $x_1^{+\phi}$ )
- $Z := (X_1^{+\phi}, X_0, \mathcal{T}, \mathcal{A})$

Much of the flexibility in controlling the nature of the flow trajectories comes from flexibility in choice of the above distributions.

### 3.2 Conditional Paths

We then construct conditional paths where elements of the state space evolve along branches of our trees. To do this, each element must track which branch on which tree it belongs to, and so we augment the state space with a branch indicator  $g_t$ . We thus have  $\tilde{X}_t := (X_t, G_t) \sim p_{t|Z}(\text{d}(x, g) | z)$  that begins at  $\tilde{x}_0 := (x_0, g_0)$  and terminates at  $\tilde{x}_1 := (x_1, g_1)$ , where at any  $t$  each element can split into two, or be deleted, depending on the trees  $\mathcal{T}$  in  $Z$ .

We identify a branch with the node ‘ahead’ of it (in the root-to-leaf,  $t = 0$  to  $t = 1$  direction), and  $g_t^{(i)} = (\tau_t^{(i)}, b_t^{(i)})$  stores a tree index  $\tau_t^{(i)}$ , and a branch indicator vector  $b_t^{(i)}$  comprising a possibly-empty ordered sequence of child indices  $\uparrow$  (first child) or  $\downarrow$  (second child) which, since the tree is binary, read from root towards leaves identifies a single branch on the tree by identifying which of the two children are descended at each bifurcation. An element of the augmented state reads  $\tilde{x}_t^{(i)} = (x_t^{(i)}, g_t^{(i)}) = (x_t^{(i)}, (\tau_t^{(i)}, b_t^{(i)}))$ . With  $\langle \rangle$  the empty branch indicator tuple (using non-standard tuple brackets to make the tuple nesting easier to read),  $(\tau_t^{(i)} = k, b_t^{(i)} = \langle \rangle)$  denotes the root of the  $k^{\text{th}}$  tree, and  $(\tau_t^{(i)} = k, b_t^{(i)} = \langle \uparrow \downarrow \rangle)$  would denote the second child of the first child of the first child of the root of the  $k^{\text{th}}$  tree.

Let  $\tilde{x}_t^{(i)} = (x_t^{(i)}, (\tau_t^{(i)}, b_t^{(i)}))$ . We use  $\triangleright$  to denote the append operation

$$\tilde{x}_t^{(i)} \triangleright \uparrow := (x_t^{(i)}, (\tau_t^{(i)}, b_t^{(i)} \triangleright \uparrow)),$$

and analogously define  $\tilde{x}_t^{(i)} \triangleright \downarrow$ .

For a state  $\tilde{x}_t = (\tilde{x}_t^{(1)}, \dots, \tilde{x}_t^{(n)})$ , we define a ‘split operator’:

$$\text{split}_i(\tilde{x}_t) := (\tilde{x}_t^{(1)}, \dots, (\tilde{x}_t^{(i)} \triangleright \uparrow), (\tilde{x}_t^{(i)} \triangleright \downarrow), \dots, \tilde{x}_t^{(n)}).$$

This duplicates, in place, the element  $\tilde{x}_t^{(i)}$ , sending a copy down each of the two child branches. We also define a ‘deletion’ operator:

$$\text{del}_i(\tilde{x}_t) := (\tilde{x}_t^{(1)}, \dots, \tilde{x}_t^{(i-1)}, \tilde{x}_t^{(i+1)}, \dots, \tilde{x}_t^{(n)}).$$

that deletes the element  $\tilde{x}_t^{(i)}$  at index  $i$ .

Between split events, each element evolves along the branch it is associated with independently of the other elements according to the chosen ‘base’ generator but conditioned to terminate, were it to reach  $t = 1$ , at the anchor  $a_i$  of the node ahead of it.

For each element, the instantaneous split event rate is just as in our counting flow described above, where a split hazard distribution  $H_{\text{split}}$  is chosen, but with  $w_i - 1$  remaining splits to be realized by  $t = 1$ . The split event intensity is thus  $h_{\text{split}}(t) \cdot (w_i - 1)$ . Similarly, a deletion hazard distribution  $H_{\text{del}}$  is chosen, and the deletion event intensity is  $h_{\text{del}}(t)$  on branches associated with deleted leaves, but 0 on branches associated with internal and surviving terminal nodes.

Since the hazard rates are designed such that all splits and all deletions implied by  $\mathcal{T}$  will be consumed by  $t = 1$ , and since the anchors  $a_i$  of all surviving terminal nodes are equal to the elements of  $x_1$ , we thus have a conditional path  $x_t \sim p_{t|Z}(x_t | z)$  that begins at  $x_0$  and terminates at  $x_1$  with probability 1.

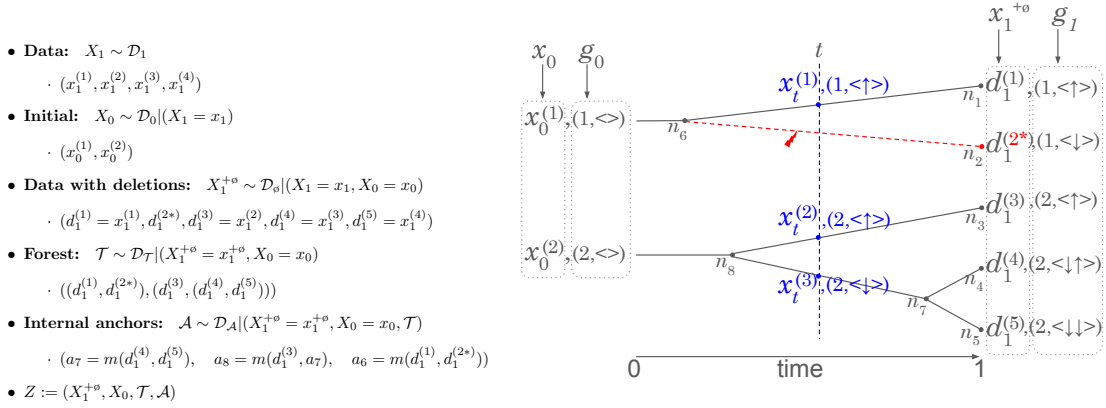


Figure 2: **Branching Flows construction.** Left outlines the sampling of  $Z$  when  $x_1$  has 4 elements and  $x_0$  has two elements, for a conditional bridge that will incur a single deletion. Right depicts the conditional sampling of  $x_t|Z$ , where elements can split and be deleted but only, in the conditional path, according to the pre-determined branching structure of the two trees  $\mathcal{T}$  in  $Z$ .

See figure 2 for a depiction of  $Z$  and the conditional path construction.

Let  $\tilde{\mathcal{E}}$  denote the augmented component-wise state space, and recall that each component-wise state space is simply  $\mathcal{E}$ . In the future, e.g., when describing conditional paths and the loss, we will denote  $\tilde{x}_t \in \prod_{n \geq 1} \tilde{\mathcal{E}}^n$  and  $\tilde{X}_t$  for a  $\prod_{n \geq 1} \tilde{\mathcal{E}}^n$  valued random variable in the main text, while in the appendix we may omit the decoration for brevity of notation.

### 3.3 Sampling from the Conditional Path

For training, we need samples at time  $t$  from the conditional path  $\tilde{X}_t \sim p_{t|Z}$ . With Branching Flows, even though the element evolution along a branch for the conditional paths is independent of the other elements, because of the branching structure the distribution of the element *value* at any given time is not. This prevents us from adopting the usual strategy for flow matching which draws conditional samples for each element independently.

However we can efficiently sample the waiting time until the next split or deletion event. If we additionally have an efficient per-element sampler for  $p(\tilde{x}_v^{(k)} | \tilde{x}_s^{(k)}, a_k)$ , where  $s < v$  and  $a_k$  is the anchor associated with the node ahead of  $\tilde{x}_s^{(k)}$ , then we can sample from the conditional path at  $t$  by recursively sampling the waiting time until the next split or deletion event, and then sampling the value of the element at the next split event (or at  $t$  if the next split event is after  $t$ ).

For the base process in our empirical examples below, we use an Ornstein–Uhlenbeck (OU) like process with time-inhomogeneous diffusion, and with mean-reversion towards the anchors, where the endpoint conditioned distribution  $p(\tilde{x}_v^{(k)} | \tilde{x}_s^{(k)}, a_k)$  follows from the results in Albano and Giorno (2020). For our discrete states we use an instance of Discrete Flow Matching (DFM) corresponding to equation 10 in Gat et al. (2024), which includes unmasking and uniform noise.

### 3.4 Handling branch indicators

Under Augmented Generator Matching, the conditional process must be Markov in  $\tilde{X}_t = (X_t, G_t)$ . Since the conditional generator is conditioned on  $G_t = g_t$ , the model parameterization of the generator must depend on  $t, x_t, g_t$ , which means that it must explicitly consider the branch indices. This seems architecturally complex at first, since these are variable length sequences, one per element of  $x_t$ . But since the sequence is ordered (and the model already knows the sequence order via positional encoding) and the trees are planar, knowing the tree and branch indicators is equivalent to knowing, between any two elements, the number of tree nodes

that they have in common along the path back to  $t = 0$ . This is simply a pairwise count matrix, which can be exposed to the model via e.g. pair features, or pair bias terms in the transformer attention mechanism.

We can instead, however, exploit Auxiliary Generator Matching and marginalize over  $G_t$ . The only change is that the branch indicator is not exposed to the model during training. The state is associated with the correct branch during the conditional process (to link it to the correct anchor for the training objective), but the model is unable to see the history of the branching tree up to time  $t$  via the branch indicator. Dropping explicit branch tracking simplifies the model architecture and the bookkeeping required during inference, which would otherwise have to track the tree that is constructed by the sequence of split and deletion events, and all of our empirical results use this Auxiliary Generator Matching version of Branching Flows.

### 3.5 Parameterization of the Generator and Loss

The base element generator is constructed as desired. For the split rate and the deletion rate, just as described for Counting Flows and Deletion Flows above, we frame these as “ $X_1$ -prediction”, and have the model predict the expected number of splits ahead of the current element by  $t = 1$ , and the probability of deletion by  $t = 1$ .

The Conditional Branching Flows (CBF) loss is the sum of three Bregman divergences: one for the base process, one against the split intensity, and one against the deletion intensity:

$$L_{\text{CBF}}(\theta) = \mathbb{E}_{t \sim \mathcal{D}[0,1], Z \sim p_Z, (X_t, G_t) \sim p_{t|Z}(d\tilde{x}|z)} \left[ D_{t, X_t}^{\text{split}}(R_t^{Z, G_t}(X_t), R_t^\theta(X_t)) + D_{t, X_t}^{\text{del}}(\rho_t^{Z, G_t}(X_t), \rho_t^\theta(X_t)) + D_{t, X_t}^{\text{base}}(F_t^{Z, G_t, \text{base}}(X_t), F_t^{\theta, \text{base}}(X_t)) \right].$$

Concretely, we use an elementwise loss where we denote  $R_{t,i}^{Z, G_t}(X_t)$  for the number of split increments ahead of the  $i$ 'th component, and  $\rho_{t,i}^{Z, G_t}(X_t) \in \{0, 1\}$  for the  $i$ 'th component of  $\rho_t^{Z, G_t}(X_t)$ . These are parametrized by  $R_{t,i}^\theta(X_t) \in (0, \infty)$  and  $\rho_{t,i}^\theta(X_t) \in (0, 1)$  respectively. We assume that the base parameterization can be written along each component as  $F_{t,i}^{Z, G_t, \text{base}}(X_t)$ .

The loss for the splitting increments mirrors that from Counting Flows (section 2.3.1), and deletions from Deletion Flows (section 2.3.2), while the base process depends on the specific application. Our chosen loss is the following:

$$L_{\text{CBF}}(\theta) = \mathbb{E}_{t \sim \mathcal{D}[0,1], Z \sim p_Z, (X_t, G_t) \sim p_{X_t, G_t|Z}(dx, dg|z)} \left[ \sum_{i=1}^{N_{X_t}} \left( R_{t,i}^\theta(X_t) - R_{t,i}^{Z, G_t}(X_t) \log R_{t,i}^\theta(X_t) \right) + \sum_{i=1}^{N_{X_t}} \left( -[\rho_{t,i}^{Z, G_t}(X_t) \log \rho_{t,i}^\theta(X_t) + (1 - \rho_{t,i}^{Z, G_t}(X_t)) \log(1 - \rho_{t,i}^\theta(X_t))] \right) + \sum_{i=1}^{N_{X_t}} \left( D_{t, X_t, i}^{\text{base}}(F_{t,i}^{Z, G_t, \text{base}}(X_t), F_{t,i}^{\theta, \text{base}}(X_t)) \right) \right]. \quad (1)$$

In the above,  $F_{t,i}^{Z, G_t, \text{base}}(X_t)$  is the generator of a per-element conditional process that will terminate (by  $t = 1$ ) at the anchor  $a(i, Z, G_t)$ , which is the anchor at the end of the branch along which the  $i$ -th component of  $X_t$  is evolving (tracked by the branch indicator of the  $i$ -th component of the augmented state  $\tilde{X}_t$ ).

### 3.6 Training

Training proceeds exactly as is standard in flow matching, by stochastic gradient descent, but with a latent  $G_t$  steering the conditional paths. We draw  $t \sim \mathcal{D}$ ,  $X_1 \sim q$ ,  $Z \sim p_{Z|X_1}$ , and then draw  $\tilde{X}_t = (X_t, G_t) \sim p_{t|Z}(d\tilde{x}_t|z)$ . From  $Z, X_t$ , and  $G_t$ , we recover  $R_{t,i}^{Z, G_t}(X_t)$ ,  $\rho_{t,i}^{Z, G_t}(X_t)$ , and  $F_{t,i}^{Z, G_t, \text{base}}(X_t)$ , and take gradient steps on the loss in equation (1).

### 3.7 Sampling from the Marginal Path

We sample from the marginal paths via Euler steps. A trained model outputs element-wise predictions  $R_{t,i}^\theta(X_t)$ ,  $\rho_{t,i}^\theta(X_t)$ , and  $F_{t,i}^{\theta,\text{base}}(X_t)$ . For a step size  $\Delta_t$ , we first take a step on the base process according to the model’s expected generator. For the branching and deletion part of each step, we calculate per-element split intensities  $h_{\text{split}}(t) \cdot R_{t,i}^\theta(X_t)$  and deletion intensities  $h_{\text{del}}(t) \cdot \rho_{t,i}^\theta(X_t)$ , and we sample which elements split or delete within the step. Elements with deletion events are removed, and elements with split events are duplicated in-place.

### 3.8 $Z$ sampling schemes

Here we outline concrete schemes for sampling  $Z := (X_1^{+\phi}, X_0, \mathcal{T}, \mathcal{A})$ , starting from  $X_1$ , that we use in our empirical examples below. Some datasets have elements that are naturally grouped (e.g. proteins, grouped by chain), and one can construct  $Z$  to respect these groupings, where it makes sense to do so (see section 4.3 for an example). In the case where there is only one group, all elements have the same group index. Further, if any elements are ‘fixed’ (e.g. in the protein example below, by a conditioning mask), then any elements with a fixed element between them in the sequence must belong to a different group.

#### 3.8.1 Initial Distribution: $X_0 \sim \mathcal{D}_0 | (X_1 = x_1)$

To sample  $X_0$  we need to sample the number of elements, and the state of each element. While in general the state of  $X_0$  elements can be coupled to  $X_1$ , here we only concretely explore schemes where each  $X_0$  element is independently sampled from a base distribution, which is a ‘masked token’ for all discrete state components, a standard isotropic Gaussian for all continuous components, and uniform samples on  $\text{SO}(3)$  for rotations.

To sample the  $X_0$  length, we use:

$$\ell_0^{\text{group}} \sim 1 + \text{Poisson}(\lambda_{\text{group}}),$$

where in many cases  $\lambda_{\text{group}}$  is 0, meaning  $X_0$  starts with a single element (or one per group).

#### 3.8.2 Deletions: $X_1^{+\phi} \sim \mathcal{D}_\phi | (X_1 = x_1, X_0 = x_0)$

Sampling  $X_1^{+\phi} \sim \mathcal{D}_\phi | (X_1 = x_1, X_0 = x_0)$  includes how many ‘to-be-deleted’ elements are introduced, where they are introduced in the sequence, and what their state is, all which can be flexibly chosen. In what we think will provide a better learning target, we consider schemes where elements of  $X_1$  are duplicated, and their state copied. In some cases it also might sense to modify the state, such as enforcing that ‘to-be-deleted’ discrete states are always masked tokens.

Importantly, deletions are chosen such that  $\ell_1^{\text{group}} \geq \ell_0^{\text{group}}$  for all groups. To ensure this, one scheme we use is to specify a deletion rate  $d_r \geq 1$ , and draw the number of to-be-deleted elements with

$$\text{del}_{\text{group}} = \text{Poisson}(\max(\ell_0^{\text{group}}, \ell_1^{\text{group}})d_r - \ell_1^{\text{group}})$$

$\text{del}_{\text{group}}$  elements are then sampled, uniformly with replacement, from the elements from the matching group of  $X_1$ , and inserted, uniformly, either side of  $X_1$  template element, inheriting its state.

Another scheme we use, only when  $\ell_0^{\text{group}} = 1$ , is to take each element in  $X_1$  and duplicate it, inserting that randomly on either side.

#### 3.8.3 Forest: $\mathcal{T} \sim \mathcal{D}_{\mathcal{T}} | (X_1^{+\phi} = x_1^{+\phi}, X_0 = x_0)$

We need  $\ell_0^{\text{group}}$  trees in  $\mathcal{T}$  (i.e. one tree per  $X_0$  element). Since the trees must be planar, we adopt a backward coalescence scheme that starts with the elements of  $X_1^{+\phi}$  and uniformly selects adjacent pairs that belong to the same group, coalescing them and replacing the pair with a single node. This proceeds until there are only  $\ell_0$  remaining elements, which become the root of each tree that is associated, maintaining the order, with the elements of  $X_0$ .

### 3.8.4 Internal Anchors: $\mathcal{A}^T \sim \mathcal{D}(X_1^{+\phi} = x_1^{+\phi}, X_0 = x_0, \mathcal{T})$

From the root to the leaves of the tree, the elements are drifting towards a sequence of anchors, which change each time a split event occurs. Thus care must be taken when sampling the anchors to maximize the learnability of the generator. One useful approach is to specify an anchor merging distribution  $p(a_{\text{parent}}|a_{\text{child}_1}, a_{\text{child}_2}, \mathcal{T})$  and recursively sample the anchors from leaves to root. Since ordered sequences of continuous values (especially for spatial positions) often exhibit strong autocorrelation with similar values for neighbouring elements, but discrete values typically do not, the anchor merging schemes differ depending on whether the state components are continuous (including manifolds) or discrete:

- Continuous: Geodesic interpolation between  $a_{\text{child}_1}$  and  $a_{\text{child}_2}$ , optionally weighted by the number of descendants of each child.
- Discrete: All internal anchors are set as a mask/dummy token.

An alternative choice which we have explored, but not used in our examples below, is copying a random child (with probability optionally weighted by some function of the number of descendants of each child).

## 4 Results

We consider three datasets: i) small molecules, where we jointly generate atom positions and atom labels, ii) Antibody heavy chains (discrete sequence only), and iii) protein backbones, comprising amino acid ‘frames’ (Jumper et al., 2021) with Euclidean positions &  $SO(3)$  orientations, and discrete amino acid sequence labels.

We are interested in understanding the degree to which Branching Flows-trained models can learn the data distribution. A strategy we use for QM9 and antibody heavy chains is to consider a set of domain-specific projections from the sample space to a scalar dimension, and then compare 10,000 Branching Flows samples to 10,000 samples from the data distribution. We also use UMAP (McInnes et al., 2020) (or seqUMAP, Hanke et al. (2022) for the antibody sequence case) for projections into two dimensions which can then be used to visualize the sample and data distribution.

### 4.1 QM9

QM9 (Ramakrishnan et al., 2014) contains small organic molecules selected from the GDB (Generated Database) chemical space enumeration. For each molecule, the 3D geometry was relaxed with density functional theory, and a consistent set of quantum mechanical properties were computed. Here we use Branching Flows to build a generative model over the atom coordinates and discrete labels (i.e. we do not consider the molecule properties).

#### 4.1.1 Data

We use a QM9 version with 130,831 molecules (Ramakrishnan, 2024), where the atom order in the coordinate files is arranged to match the canonical SMILES string ordering, where hydrogens are (almost always) after the heavy atoms. We reasoned that the splitting mechanism of Branching Flows would not excel if there are spatially distant elements that are neighbors in the primary sequence, since a late split would then require very large flow velocities. We thus kept the primary heavy atom ordering (since neighboring SMILES atoms are often bonded, and thus spatially close), but redistributed the hydrogens such that each hydrogen is inserted into the sequence in front of its nearest heavy atom, ordered by distance when there are more than one hydrogen neighbour per heavy atom.

#### 4.1.2 Branching Flows specification

For QM9, we constructed our Branching Flow with the following choices:

- Conditional base process:
  - Continuous: OU process flow (Appendix C), with a mean-reversion rate  $\theta = 5$ , and where the variance decays from 10 when  $t = 0$  to 0.001 by  $t = 1$ .

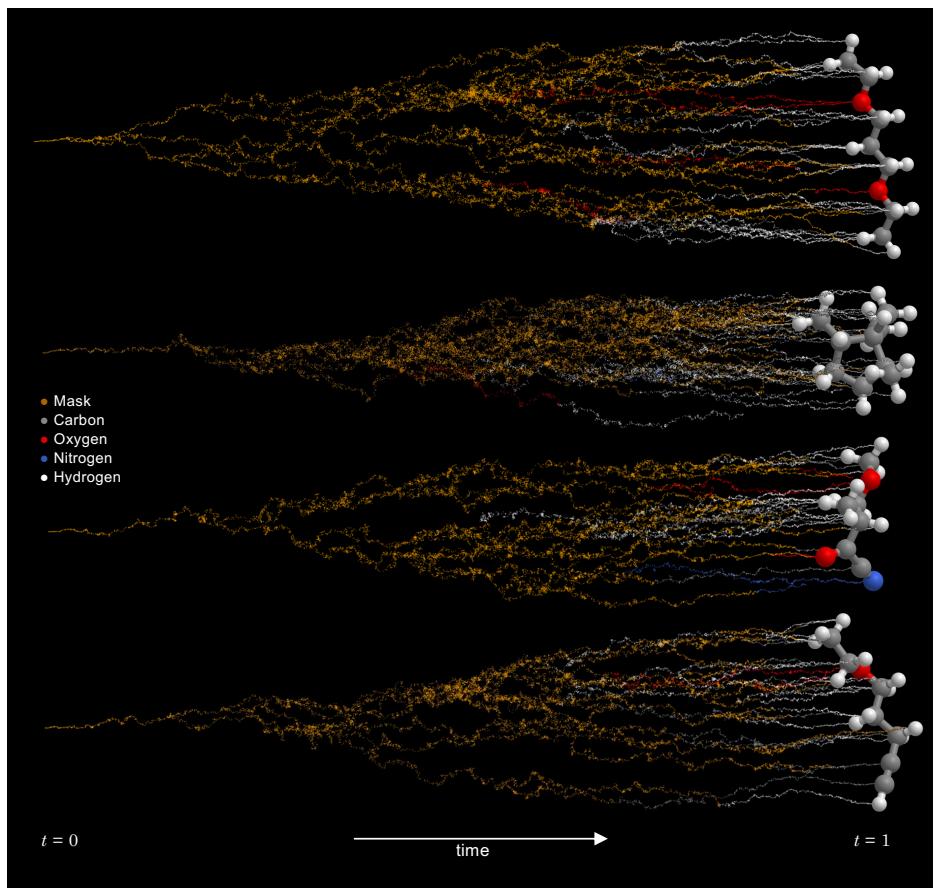


Figure 3: **QM9 Branching Flows sampling trajectories.** A visualization of inference trajectories from a QM9-trained Branching Flows model. The final sampled molecule, when  $t = 1$ , is depicted on the right. At every inference step from  $t = 0$  to  $t = 1$ , we draw the current  $x_t$  state as colored points, with a small rightward displacement, which shows the branching and deletion history as  $x_t$  is transported from a single element when  $t = 0$  to the final sampled molecule. The color of the trails shows the atom type which begins as ‘Mask’ (in orange) and switches to concrete atoms as  $t \rightarrow 1$ . For the purposes of visualization we use 2000 steps with a modified step schedule:  $t = (1 - (\cos(s\pi/2)))$ , for  $s \in (0, 1/2000, 2/2000, \dots, 1)$ .

- Discrete: DFM convex interpolation of  $x_0$ , uniform noise, and  $x_1$ , with hazards  $\mathcal{D}_1 = \text{Beta}(2, 2)$ ,  $\mathcal{D}_2 = \text{Beta}(2, 2)$ ,  $\omega_u = 0.2$ .
- Branching hazard distribution:  $\text{Beta}(1, 3/2)$
- Coalescence policy: uniformly merge adjacent nodes.
- Deletion hazard distribution:  $U(0, 1)$
- To-be-deleted policy: Each element of  $x_1$  gets duplicated and the to-be-deleted duplication is inserted (with equal probability) immediately before or after the original element.
- $x_0$  state distribution:  $N(0, 1)$  for each continuous coordinate, and mask/dummy token for the discrete atom label.
- $x_0$  length distribution: 1, always.

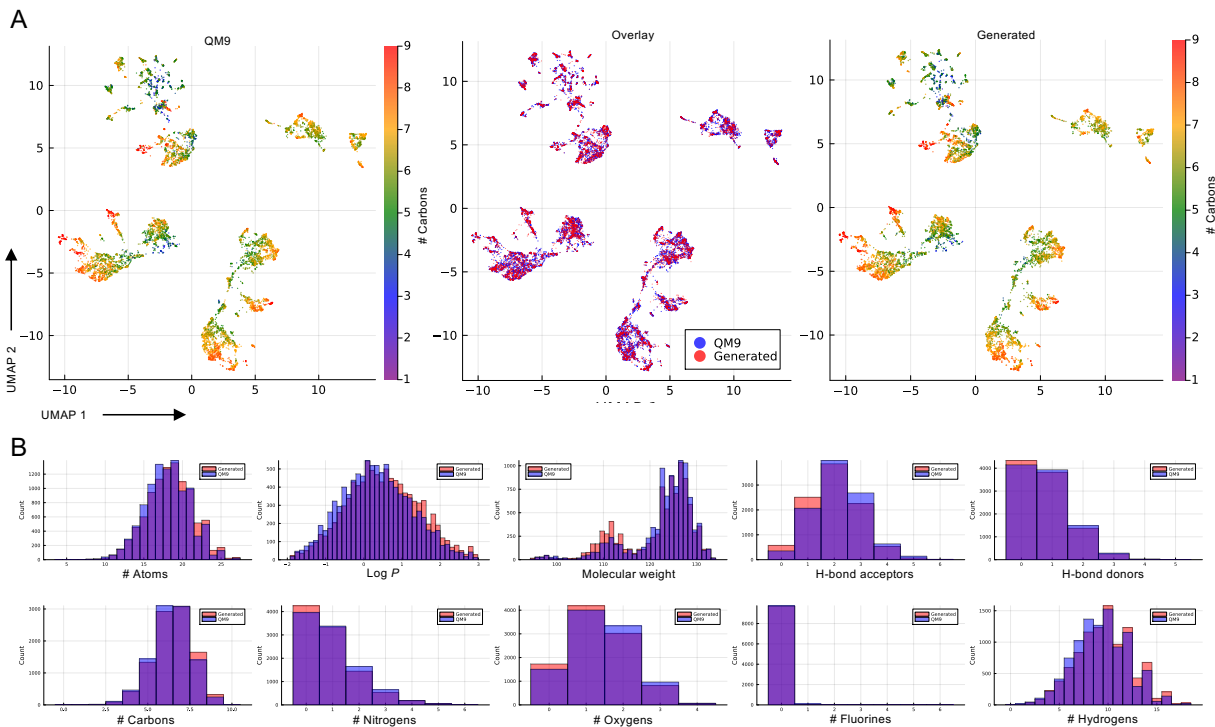


Figure 4: **QM9 data vs generated samples.** 10,000 random samples from the QM9 dataset vs 10,000 samples generated using a Branching Flows model. Panel A computes molecular fingerprints (using RDKit) and jointly embeds QM9 data and generated samples using UMAP. Left shows QM9-only embeddings, colored by the number of carbon atoms in each molecule; right shows generated samples, similarly colored, and center shows the overlap of QM9 (blue) vs Branching Flows generated samples (red), showing similar distributions. Panel B depicts univariate property distributions from QM9 and Branching Flows generated samples, including atom counts, as well as a number of standard molecular descriptors computed with RDKit.

### 4.1.3 Model and Training

We use a 12 layer transformer model (12 heads, each with head dimension of 64), with an embedding dimension of 384. The atom positions are encoded by Random Fourier Features (RFFs), and pairwise spatial features are also provided to each layer by a learnable, layer-specific, head-specific attention bias. Rotary Positional Encoding (RoPE, Su et al. (2023)) is used to encode the primary sequence ordering. The final six layers additively update the atom positions (and the spatial pair features are recalculated after each position update). The model outputs the endpoint-predicted (i.e. by  $t = 1$ ) locations, logits over the endpoint-predicted discrete state, the log of the per-element expected number of future bifurcations by  $t = 1$ , and a deletion binary logit. The model was trained, using Muon (Jordan et al., 2024) with post-warmup learning rate of 0.005, for 500k batches (where each batch was 128 randomly-sampled QM9 molecules) and a linear learning-rate cooldown for the last 50k batches.

### 4.1.4 Results

Figure 3 shows typical inference trajectories for QM9 molecules. Starting from a single  $x_0$  element with a random position and a masked label, the process undergoes a sequence of bifurcations and deletions governed by the rates output from the model, with the discrete states switching along the trajectory as well, terminating at a generated molecule.

The only relevant benchmark for our purposes is whether the model learns, via Branching Flows, to sample from the data distribution. To investigate this, we generated 10k samples and compared these to 10k QM9 samples (See appendix E.1 for details).

Figure 4 compares generated and data distributions for molecule fingerprints, which encode molecule properties into a fixed-length bit vector, embedded into two-dimensions by UMAP, showing no apparent differences. Also shown are univariate histograms of atom counts and molecule properties, with some subtle departures, most visible in  $\text{Log}P$  and molecular weight.

We also compare 10,000 samples from a QM9-trained ‘Transdimensional Jump’ diffusion model (Campbell et al., 2023). We use a Kolmogorov-Smirnov based statistic ( $1 - KS_D$ ; see appendix E.1) to quantify agreement between the samples and the data distribution, as shown in table 1. For all univariate metrics, Branching Flows better matches the data distribution. We explore these differences further with visualizations in appendix figure 10.

Model	mw	logp	hbd	hba	C	H	O	N	F	atoms
Branching Flows (ours)	0.9091	0.9276	0.9876	0.9259	0.9638	0.9408	0.9589	0.9672	0.9946	0.9457
Transdimensional Jumps	0.8867	0.8319	0.8726	0.8407	0.8144	0.8553	0.9316	0.8645	0.9678	0.8690

Table 1: Distribution agreement ( $1 - KS_D$ , higher is better) between univariate properties of samples from each model vs. QM9 data. From left to right: Molecular weight, LogP, hydrogen-bond donors, hydrogen-bond acceptors, number of: carbons, hydrogens, oxygens, nitrogens, fluorines, and the total number of atoms.

## 4.2 Antibody Sequences

To investigate Branching Flows on a pure discrete sequence learning task, we consider the problem of antibody amino acid sequence generation. Antibodies exhibit substantial length variation, most concentrated in the complementarity determining regions (CDRs) which are the primary determinants of antibody-antigen interaction. They originate from a stochastic recombination of variable, diversity, and joining germline gene segments, with non-templated junctions in between, and then further diversify via somatic hypermutation (Murphy and Weaver, 2016).

Here we compare a Branching Flows model to an ‘oracle-length’ discrete flow matching model, which is identical to the Branching Flows model except that it i) has no splits or deletions, and ii) is initialized with a ‘true’ length sampled from the data distribution. We also attempted to implement Edit Flows (Havasi et al., 2025) for comparison.

### 4.2.1 Data

Antibody sequence models were trained on a filtered subset Turnbull et al. (2024) of the antibody heavy chains from the Observed Antibody Space database (OAS) (Kovaltsuk et al., 2018). The filtering retained only human sequences and removed sequences with unknown residues, missing conserved cysteines and those which had framework region 1 or 4 shorter than allowed by IMGT definitions. Sequences were further filtered to remove redundancy by clustering at 95% identity. This resulted in a total of 118 million sequences, of which a random subset of 15 million were sampled and used for training. For the evaluation of the model, a similarly-filtered subset of the OAS data was used.

### 4.2.2 Branching Flows Specification

- Conditional base process:
  - Discrete: DFM convex interpolation (appendix B) of  $x_0$ , uniform noise, and  $x_1$ , with hazards  $\mathcal{D}_1 = \text{Beta}(1.5, 1.5)$ ,  $\mathcal{D}_2 = \text{Beta}(2, 2)$ ,  $\omega_u = 0.2$ .
- Branching hazard distribution:  $\text{Beta}(1, 2)$
- Coalescence policy: uniformly merge adjacent nodes.
- Deletion hazard distribution:  $U(0, 1)$
- To-be-deleted policy: deletion rate  $d_r = 1.2$

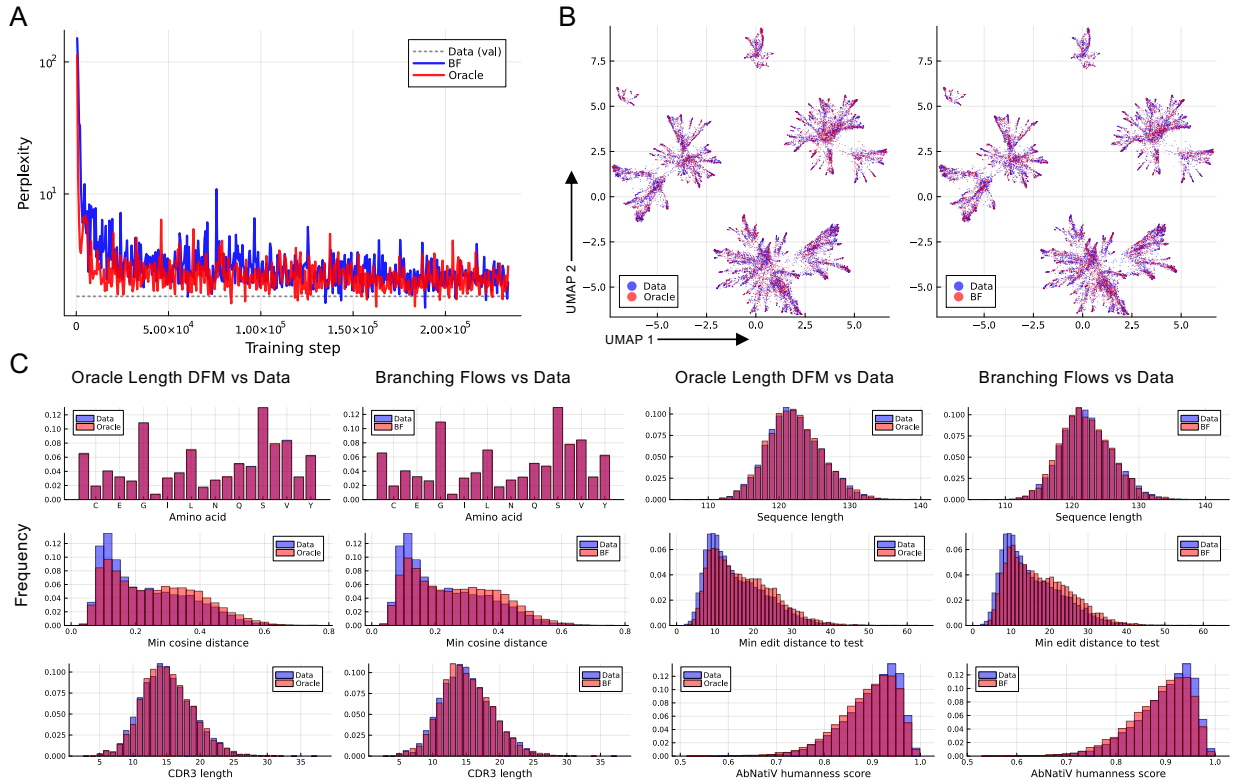


Figure 5: **Antibody generation distribution matching.** **A** The perplexity, evaluated under an autoregressive LLM, of samples generated by Branching Flows vs an oracle-length discrete flow matching model (where the length for each sample is taken from a random real sequence). This is shown over training iterations. **B** two seqUMAP (Hanke et al., 2022) plots comparing the clustering of real data with the oracle-length samples and the Branching Flows samples, respectively. **C** Comparison of several distributions of the generated sequences with sequences from the validation data set.

- $x_0$  state distribution: masked tokens.
- $x_0$  length distribution: uniform between 110 and 140.

### 4.2.3 Model and Training

For the antibody sequence modeling task, we used a transformer-based architecture similar to that of a diffusion transformer (Peebles and Xie, 2023), but with additional split and deletion heads. Time was embedded with RFFs, and adaptive layer normalization (adaLN-Zero) was used for time conditioning. The model had an embedding dimension of 768, 12 attention heads, and 8 layers.

The models (Branching Flows, oracle-length and Edit Flows) were trained using a batch size of 64 resulting in a total of 234 375 training steps for the 15 million sequence dataset. Muon was used with a 2000 step linear warm-up followed by a cosine decay starting at  $10^{-3}$  and decaying to  $10^{-7}$ .

### 4.2.4 Results

Figure 5 shows the distributions of statistics (Appendix E.2) from antibody sequences generated by both the Branching Flows and oracle-length models. It also includes the perplexity-over-time plot and 2 seqUMAP (Hanke et al., 2022) representations of the 10 000 generated sequences. Generally, these plots show that distributional overlap with natural sequences is similar between Branching Flows and the oracle model, despite the oracle having additional information. As both models were only trained on 15 million sequences, we

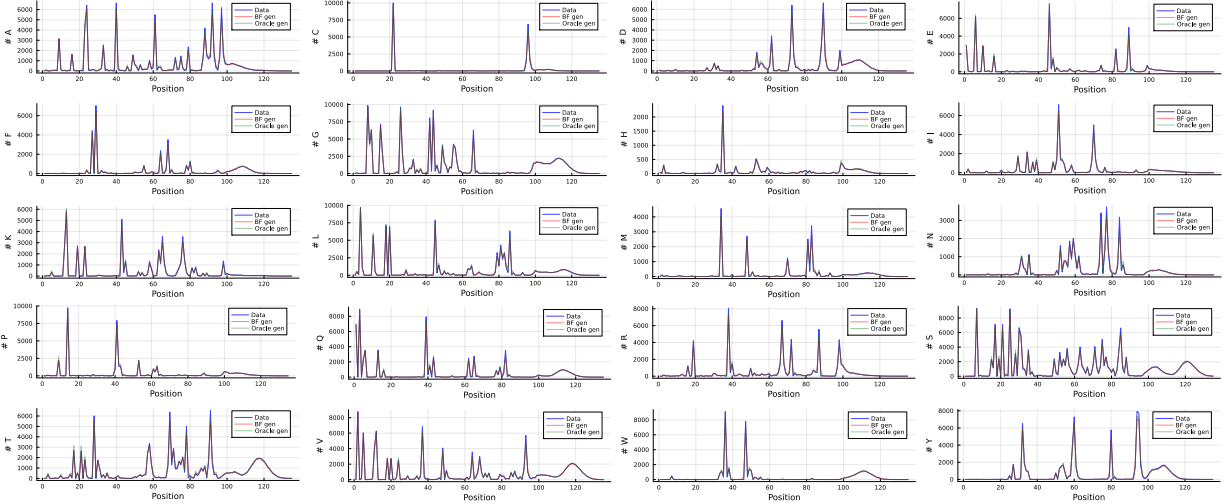


Figure 6: **Amino acid position distributions.** The count of the number of each amino acid at every position in natural data, and in samples from Branching Flows (‘BF gen’) and Oracle Length DFM (‘Oracle gen’).

anticipate that further training will improve the distributional match. Finally, we plot the sequence-position-specific amino acid frequency distributions for all 20 amino acids in figure 6, which shows that Branching Flows can learn strong position dependence despite not having any prior information about total length.

Table 2 shows distribution matching statistics for the three models. In general, Branching Flows and the Oracle length model are very close across all metrics. Edit Flows performs well at length matching (both total and CDR3 length), but has lower distribution matching performance for metrics that consider the content of the generated sequences. SI figure 11 explores these in more detail.

Method	Length	Diversity	Novelty	CDR3 length	AbNatiV
Oracle length	0.995	0.899	0.903	0.984	0.943
Branching Flows (ours)	0.986	0.894	0.888	0.989	0.931
Edit Flows	0.989	0.713	0.770	0.983	0.769

Table 2: Distribution agreement ( $1 - KS_D$ , higher is better) between univariate properties of samples from each model vs. validation sequences. From left to right: Sequence Length, Diversity (within-samples min Cosine distance), Novelty (minimum edit distance to true sequence), CDR3 length, and AbNatiV ‘humanness’ score.

### 4.3 Multimodal Branching Flows for Protein Structure and Sequence Generation

To investigate whether Branching Flows would scale to a more complex learning problem where the state space is multimodal, we modified and finetuned a pre-trained ChainStorm model (Oresten et al., 2025) to allow the model to determine how long chains, or designable segments, should be.

Briefly, ChainStorm is a multimodal flow matching model that jointly generates protein backbones and amino acid sequence labels (but not side chain atom positions). Amino acid backbones are represented as sequences of ‘frames’ (Jumper et al., 2021) with Euclidean positions and  $SO(3)$  rotations, and ChainStorm uses an Invariant Point Attention (Jumper et al., 2021) transformer architecture to estimate the  $t = 1$  frame positions and orientations, whose conditional/marginal paths are governed by Euclidean Brownian Motion and  $SO(3)$  rotational diffusion. Discrete Flow Matching (Gat et al., 2024) is used for amino acid sequence labels.

ChainStorm’s Euclidean and  $SO(3)$  conditional processes were constructed with relatively low noise, but we reasoned that Branching Flows, especially with late-time branching events requiring higher flow velocities,

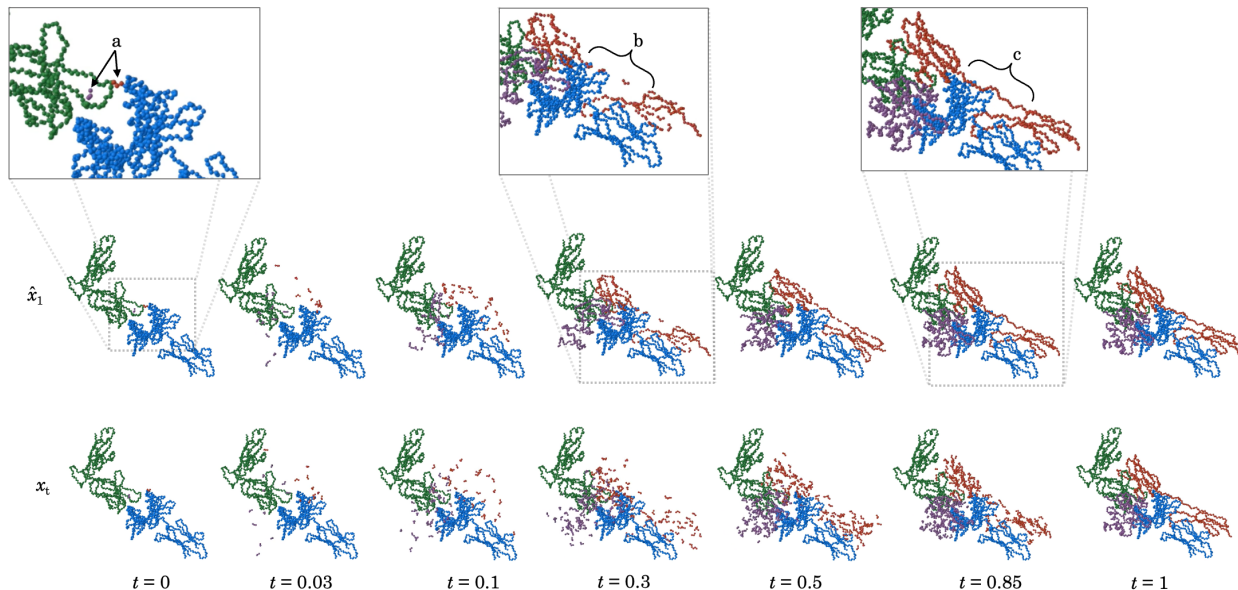


Figure 7: **Branching Flows protein sampling trajectories.** Shown are snapshots from a sampling trajectory from BF-ChainStorm, with both the current state  $x_t$  and the model’s prediction of the end state,  $x_1$ . The trajectories are colored by chain, and each backbone residue is shown as three spheres ( $N, C\alpha, C$ ). Here, two chains were fixed, and two chains were designable, with each designable chain starting from a single residue (arrow a in the first inset). The chains grow over time, and in this example the orange chain converges on two separate domains. Interestingly, during the intermediate flow state ( $t = 0.3$ , bracket b in the second inset), as the two domains resolve in  $x_1$ , they are not connected to each other, and the model uses split events to build a complete linker between them by  $t = 1$ .

might benefit from noisier processes which would have higher flow velocities generally, so we first finetuned a ChainStorm model with modified element-wise conditional processes, using

- for Euclidean positions, a time-inhomogeneous OU process with mean reversion rate of 100, and a variance of 150 at  $t = 0$  that decays to 0 as  $t \rightarrow 1$ .
- for  $SO(3)$  rotations, a manifold-respecting version of the above OU process with identical parameters.
- for discrete states, a DFM convex interpolation (appendix B) with a  $\mathcal{D}_1 = \text{Beta}(3.0, 1.5)$ ,  $\mathcal{D}_2 = \text{Beta}(2, 2)$ ,  $\omega_u = 0.2$ .

All Branching Flows protein models were then finetuned atop this model, which exhibited much higher variance sampling paths than the original ChainStorm.

We then modified the ChainStorm architecture to construct ‘BF-ChainStorm’ to allow for i) element branching and deletion, and ii) conditioning on fixed protein components (in general any set of residues, but here chains or contiguous segments of chains) that are then prevented from changing during training or inference. Conditioning is done by including a ‘conditioning mask’ embedding layer whose outputs get summed into the initial activations, and by preventing the per-layer frame updates for fixed residues. For element branching and deletions, we reasoned that, since we are finetuning into an existing model, we didn’t want to only extract contributions from the final output layer (since this is used for rotations, positions, and discrete states), so we concatenate the output activations from the last three layers. This is summed into an embedding of  $t$  and that sum is passed into a SwiGLU-like layer that collapses to a single dimension. This is done separately for branching and deletion, and the outputs are interpreted as ‘logits’ for loss (during training) and rates (during inference). Finally, since the state dimension now changes during inference, we replaced ChainStorm’s self-conditioning with recycling, which requires no architectural changes but instead requires additional model passes within each inference step.

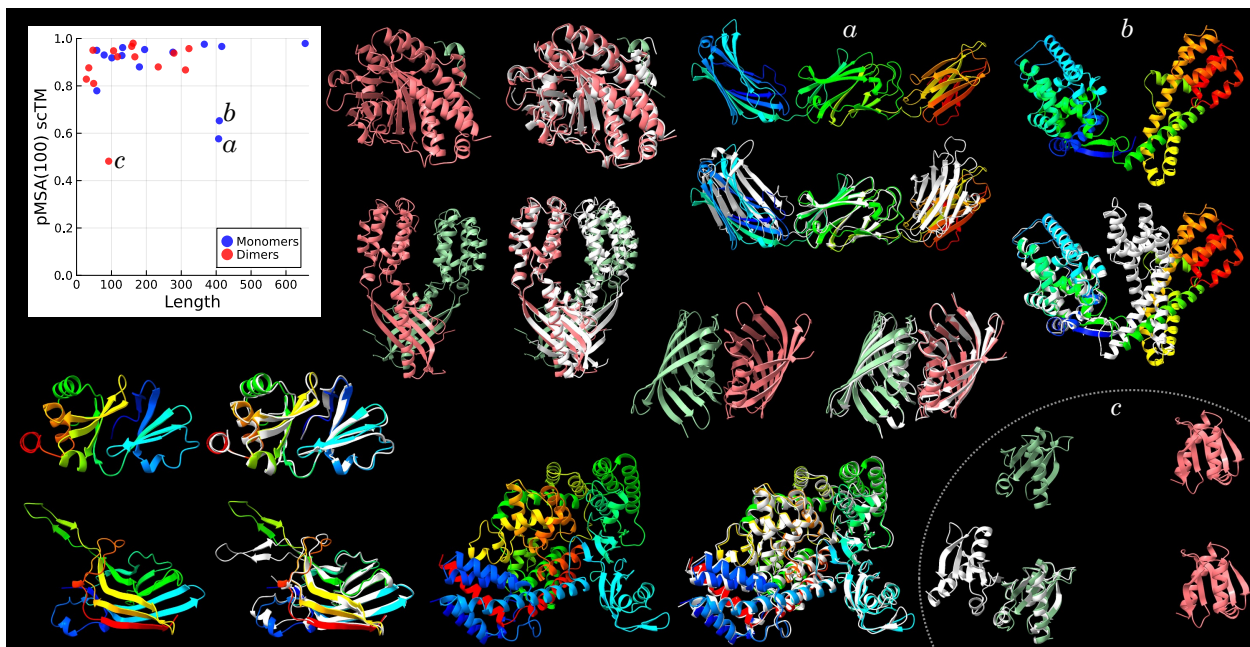


Figure 8: **Branching Flows protein samples.** Top left inset shows pseudoMSA scTM refolding scores, and selected samples are shown (rainbow colored for single chains, and per-chain for dimers). To the right or below each is shown an overlay of the sample and the refolded structure (grey). Specifically, the three worst scTMs are depicted (labelled a, b, and c on the inset and the main panel, showing that the low scTMs are driven by unpredictability due to flexible linkers, or incorrect dimerization prediction.

One subtlety related to Branching Flows is that, originally, ChainStorm conditioned on residue indices which provide, during training, the model with information about when parts of backbone are missing (i.e. unresolved in the crystal or cryo-EM structures) since a gap in the residue numbering will be present. To generate backbones without ‘chain breaks’ (usually the desired behavior), at inference time the generation is conditioned on residue numbers with no gaps. However, since BF-ChainStorm’s conditional/marginal paths change by insertions and deletions with  $t$ , including residue numbers no longer makes sense, as the number of residues for any intervening segment (which, in BF-ChainStorm, must be stochastically generated during inference) would be pre-determined by the residue numbering. So instead of residue indices, we use fixed-increment positional index. However, since the training data has many chain breaks, the model would then stochastically generate structures with chain breaks. So we additionally introduced a ‘break mask’ encoder (also summed into the starting activations) that encodes, on a per-chain basis, whether the ‘designable’ portion of the chain includes any chain breaks. When used during inference, this reduces the number of chain breaks but doesn’t remove them entirely, possibly because the model is getting conflicting signals between the conditioner and the emerging structure (e.g. large unstructured loops are often not resolved in protein structures, so if the model is generating one that might overwhelm the chain-break conditioner). Chain breaks are easy to detect using bond distances, and we exclude them from refolding analysis because our folding pipeline requires intact chains.

When sampling trees  $T$  for protein models, when the group (described above) is the chain index, the requirement that separate chains never occur on the same tree allows the number of sampled chains in a structure to be specified at inference time (but each of their lengths stochastically sampled by the model). Similarly, any residues (even within a single chain) separated by residues fixed in the conditioning (relevant for BranchSegment) may not coalesce when sampling trees. Thus no single tree spans two designable segments.

We finetuned two models: one to generate chains (‘BranchChain’), and one to sample segments of contiguous residues (‘BranchSegment’). For BranchChain, the designable residues were always complete chains, where the chains were randomly selected for masking during training, so it can generate chains unconditionally, or it can generate chains conditioned on other fixed chains. BranchSegment’s conditioning

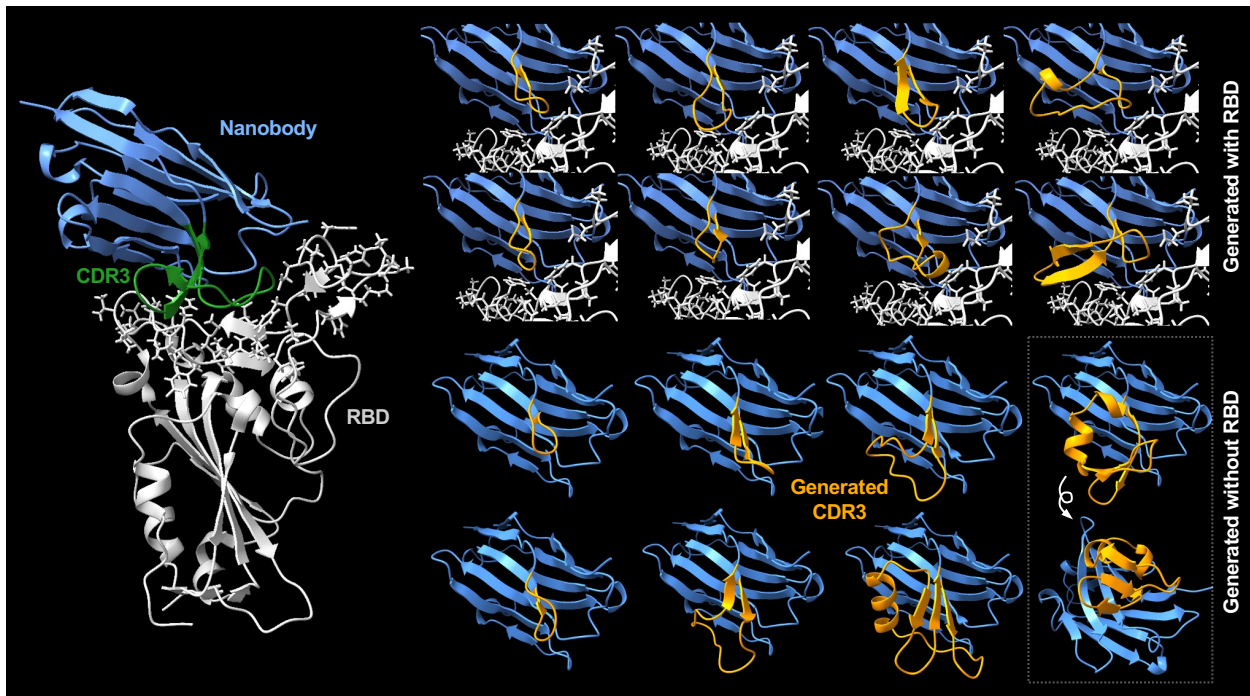


Figure 9: **Branching Flows protein ‘infix’ samples.** Depicted is the template PDB (9IQP, Shcheblyakov et al. (2025)) where only the CDR3 (green in the template) was designable, and the rest of the structure was fixed and conditioned upon. The top two rows of samples show generated CDR3s when they are generated in the context of the binding partner, and the bottom two rows show generations in the absence of the binding partner.

mask during training was a random number of random-length contiguous segments, so multiple segments can be simultaneously designed during inference.

For BranchChain, we initialize each chain to have  $1 + \text{Poisson}(20)$   $x_0$  elements, each drawn from the ChainStorm base element distribution, and for BranchSegment each designable segment has a single  $x_0$  element. For sampling ‘to-be-deleted’ elements, we use  $d_r = 1.2$  for BranchChain and  $dr = 1.1$  for BranchSegment (reasoning that the more strongly informative conditioning information for BranchSegment might require less exploratory flow paths). Samples were generated with 400 steps:  $t = 1 - (\cos(\pi\tau) + 1)/2$  for  $\tau \in (0, 1/400, 2/400, \dots, 1)$ .

For illustration purposes, we also finetuned a BranchChain variant with only a single  $x_0$  element per chain. Figure 7 shows steps along the sampling trajectory for a sample where two chains (blue and green) were fixed, and two chains were sampled. The orange chain, best seen through the lens of the model-predicted end state  $x_1^{hat}$ , highlights a key Branching Flows feature: at first, the designed chain converges upon two separate domains, with insufficient residues in between for them to be linked. This is then progressively filled in by insertions, until a complete links connects them as a single chain.

To investigate whether a Branching Flows protein model can generate samples with reasonable protein-like geometry, we sampled, without conditioning, 20 monomers and 20 dimers. Discarding samples with chain breaks (one monomer and five dimers), and samples too short for meaningful evaluation ( $< 25$  residues in the longest chain: five monomers, and 1 dimer), with 14 monomers and 14 dimers remaining. Using the ‘pseudoMSA refolding’ strategy from ChainStorm (Oresten et al., 2025), we use a state-of-the-art protein folding model and test the extent to which it can recover the generated protein geometry from sequences only, which shows that our designs have geometry consistent with the folding model. We generated a pseudoMSA of 100 sequences for each of these with ProteinMPNN (Dauparas et al., 2022), and evaluate the ‘self-consistency TM scores’ of a single refold, via Boltz2 (Passaro et al., 2025) of this pseudoMSA.

Figure 8 shows the scTM scores, most very close to 1. We also show selected examples, for monomers and dimers, of BranchChain generated proteins and their refolds, specifically showing the three cases with

low scTMs. For the two poorly refolded monomers, this is because the generated structure had one or more flexible linkers, and the individual domains were well refolded. For the poorly refolded dimer, this was because BranchChain generated two disconnected chains, and Boltz2 placed these adjacent. Further exploratory sampling suggests that BranchChain does sometimes generate disconnected chains.

Overall, BranchChain generates samples with a variety of protein chain lengths, with plausible backbone geometry. Further, as can be seen in many of the samples in figure 8, the propensity of the ChainStorm base model to sample homodimers is preserved. This is interesting given that ChainStorm’s single attention head that governs symmetric oligomer sampling is primarily driven by chain lengths which are fixed in ChainStorm, but now stochastically generated in BranchChain.

For BranchSegment we do not attempt quantitative evaluations, but we demonstrate that it is a promising solution to the ‘unknown length infix sampling’ problem. Taking a protein complex (PDB: 9IQP, Shcheblyakov et al. (2025)) of a nanobody and the SARS-CoV-2 receptor binding domain (RBD), we mask only the ‘Complementarity Determining Region 3’ (CDR3) as designable, and we generate 20 samples from the RBD-bound complex, and 20 samples from the unbound nanobody alone. The sampled CDR3s had a broad length distribution (7 to 29 residues for bound, 7 to 40 unbound). For the bound samples, even though the side chain atom positions from the RBD were not provided to BranchSegment (it only sees backbone frames and amino acid labels) the designed CDR3s had no atomic clashes with the RBD side chain rotamers for 15 out of 20 of the generated CDR3s. Some of the unbound CDR3s appear structurally plausible, but are extremely unlikely to occur naturally, which is not surprising since neither the base model nor BranchSegment have any antibody or nanobody-specific training.

## 5 Implementation, Availability, and Key Dependencies

Branching Flows is available as a Julia (Bezanson et al., 2017) package BranchingFlows.jl (<https://github.com/MurrellGroup/BranchingFlows.jl>). This composes with base processes implemented in Flowfusion.jl (<https://github.com/MurrellGroup/Flowfusion.jl>). Demos and specific models are available via <https://github.com/MurrellGroup/BranchingDemos.jl>, with protein models available at <https://github.com/MurrellGroup/BranchChain.jl>.

We rely on Flux.jl (Innes et al., 2018) for our deep learning environment, Zygote.jl for automatic differentiation (Innes, 2018), CUDA.jl (Besard et al., 2018) for GPU interaction, Makie.jl (Danisch and Krumbiegel, 2021) and Plots.jl (Christ et al., 2023) for visualization, and NNop.jl (<https://github.com/FluxML/NNop.jl>) for customized flash attention (Dao et al., 2022) kernels. For small molecule processing for the QM9 dataset, we use MoleculeFlow.jl (<https://github.com/MoleculeHub/MoleculeFlow.jl>), which wraps RDKit (<https://www.rdkit.org>). Additionally, for the protein model we rely on all the packages listed in Oresten et al. (2025).

## 6 Related Work

**Edit Flows** Havasi et al. (2025) describe Edit Flows, a method for varying-dimensionality generation of discrete sequences. Edit Flows works by parameterizing the rates of *edit operations* (insert, delete and substitute). During training, an *auxiliary alignment process* is introduced. This entails adjoining to the alphabet a null token  $\varepsilon$  such that the sequence length of  $X_0$  is the same as the sequence length of  $X_1$ . One denotes this new space by  $\mathcal{X} \times \mathcal{Z}$ . Then, transitions in this augmented space are interpreted as either insertions (swapping  $\varepsilon$  to a token in the alphabet), deletions (swapping a token in the alphabet for  $\varepsilon$ ) or a substitutions (swapping two tokens in the alphabet). The model only sees  $t$  and  $\mathcal{X}$ , and the marginal rates of a CTMC on  $\mathcal{X}$  are learnt by training against a CTMC on  $\mathcal{X} \times \mathcal{Z}$ . Edit Flow’s main contribution is proving, for the discrete case, that you can marginalize over this time-dependent latent process. In Branching Flows we sample a non-time-dependent latent that fully specifies how elements in  $X_0$  will map, via splits or deletions, to elements in  $X_1$ , allowing us to extend beyond discrete states, and affording flexibility in how the sample paths are constructed. Furthermore, to extend Edit Flows to a continuous setting one would have to parametrize and learn a flexible distribution over insertions into a continuous space, which is often hard in practice. Later, One Flow (Nguyen et al., 2025) uses the approach of Edit Flows to allow the interleaving of images and text by inserting ‘image tokens’.

**Transdimensional jumps** Transdimensional jump diffusion (Campbell et al., 2023) models continuous-valued variable-cardinality states. Between jumps, a base SDE evolves the continuous coordinates, while at jump times, the dimension changes by one. In the forward direction (data noising — diffusion models adopt the opposite convention to flow matching), one component is deleted at a specified rate, chosen such that the forward process will terminate at a single surviving component.

The time reversal of the forward process is again a jump diffusion process, but where elements are inserted into the state, and a neural network parametrizes the insertion state and post-insertion distribution of the inserted element. One challenge is that, unlike Branching Flows’s ‘split’ mechanism, the insertion distribution does not have a simple form, and any tractable approximation used in practice (e.g. a Gaussian) can cause a mismatch between the conditional and marginal process.

**DrugFlow** In Schneuing et al. (2025) a trans-dimensional model for small molecule generation is presented. It works by introducing a virtual atom type whose coordinates are set to the center of mass of the ligand and which have no bonds. During training the training data is augmented by adding  $n_{\text{virt}} \sim U(\{0, 1, \dots, N_{\text{max}}\})$  virtual nodes, to allow the model to learn to set some atom categories to the virtual category. The model is thus deletion-only and requires specifying a priori  $N_{\text{max}}$  which leads to a fixed upper bound on generated molecule size. This contrasts to Branching Flows, which can generate arbitrary-length objects and allows both insertions and deletions. Furthermore, elements in the virtual category are retained in the flow and evolve under it (although their bond types are set to ‘None’), which forces model computation to always be done on the maximum number of elements for the specific molecule being generated.

## 7 Discussion

We have shown that Branching Flows is a capable ‘distribution-learner’ of multimodal states that vary in length, addressing a previously-unsolved fundamental problem.

For now, we restrict ourselves to demonstrating new capabilities afforded by Branching Flows, without extensive comparisons on downstream tasks and benchmarks. The reason for this is that performance benefits on benchmarks are often more sensitive to practically useful but theoretically uninteresting domain-specific adjustments to the model and training details, which is orthogonal to the purpose of this manuscript.

For the QM9 small-molecule dataset, we compare samples from our Branching Flows-trained model with those from the Transdimensional Jump Diffusion model of Campbell et al. (2023), showing favorable distribution matching for Branching Flows. We suspect this difference is attributable to two things. Firstly, transdimensional jump diffusion spawns elements at a position that is, in its conditional process, coupled to an element in the data distribution. While the conditional distribution of the spawn point is Gaussian conditioned on the corresponding  $X_1$  element, the marginal distribution during inference is a (possibly infinite) mixture of Gaussians. Practically, the model must be content with a coarse approximation of this distribution, such that, even in the small step limit, there will be a mismatch between the conditional and marginal paths. Branching Flows avoids this by spawning new elements via a splitting mechanism that, conditioned on  $X_t$  is independent of  $X_1$ .

Secondly, transdimensional jump diffusion handles discrete atom types by converting them to continuous vectors, which does not compare favorably to discrete character diffusion models (Sahoo et al., 2024). Branching Flows allows composition of the branching and deletion process with any underlying flow matching base process, naturally accommodating true multimodal state spaces.

However distribution matching differences may also be attributable to model architecture differences or training details. The transdimensional jump model uses a domain-specific equivariant architecture, while Branching Flows uses a generic one, for example. A side-by-side comparison with identical architecture and training might alter the results, in either direction.

For the antibody sequence modeling problem, we show a side-by-side comparison between Branching Flows and an oracle-length model that is provided, via the number of starting tokens, the true length of the sequence. During inference, this length is sampled from the data distribution. We show that both the training dynamics of Branching Flows, and the ability to match the data distribution, are similar to a model that has been provided the true length.

Note that while training an oracle-length model might be a viable strategy for unconditional generation tasks if any data are available at inference time, sampling the length from the data distribution is not possible for conditional generation tasks (e.g. conditioning on some fixed part of the sequence), as one generally cannot *conditionally* sample length from the data distribution at test time.

Since Edit Flows (Havasi et al., 2025) allows modeling of variable length discrete sequences, it is a natural comparator for the antibody sequence modeling problem. Here the model architectures are matched between Branching Flows and Edit Flows, where the only difference is that the Edit Flows insertion head is as large as the alphabet size, whereas Branching Flows only needs one splitting rate per element. While we see favorable performance of Branching Flows, one strong caveat is that this is our own Edit Flows implementation, and not a reference implementation provided by the authors, and it is quite possible that there are implementation details that are causing this difference in performance. Another possible explanation, in line with our empirical results, is that the Edit Flows construction does not allow substitutions to be parameterized purely as logits predicting the  $X_1$  state, which might make the substitution process more difficult to learn. The anchor mechanism in Branching Flows, on the other hand, allows for direct  $X_1$ -prediction.

For our protein structure models, we do not perform extensive validation. Most standard protein benchmark metrics are problematic. For now we content ourselves in showing that Branching Flows generates samples that have geometry consistent with a state-of-the-art folding model.

In terms of capabilities, as far as we are aware ‘BranchSegment’ is the first generative model that can perform ‘unknown-length infix sampling’ for proteins, where the backbone is constrained either side of the designable region, and the length of the designed segment is determined by the model. In practice, current generative models can use a range of pre-sampled lengths, with post-sampling filters to select from these, and non-generative models can perform sequence search on a surrogate objective (e.g. via a folding model). Neither will provide distribution-matching guarantees, and both are computationally expensive. Further, the ‘pre-sampled length’ strategy required by fixed-length flow and diffusion models can combinatorically explode if there are multiple sequentially non-contiguous but spatially-interacting segments that need to be designed, which would be the case during protein-protein interface design or re-design.

One practically useful feature, demonstrated with ‘BranchChain’ and ‘BranchSegment’ is that Branching Flows can be finetuned into an existing model. A few days on a single GPU was sufficient. This suggests that, even though the base model was trained via fixed-length flow matching, the internal representations required to learn the branching and deletion process may already be present. This would be extremely useful if it extends to other models, allowing large models with high pretraining cost to be repurposed with Branching Flows.

Branching Flows is really a family of methods whose behavior will differ depending on the strategies used to construct the trees and the anchors. Currently, we use the simplest ‘uniform adjacent merge’ tree sampling strategy, with some domain-specific tweaks like preventing merges between elements from different protein chains. We anticipate that domain-specific tailoring of this will be generally useful to constrain the Branching Flow trajectories, as many problems have a natural tree-like structure. For example for ‘code generation’, which is a discrete sequence modeling problem, the trees could be sampled to mirror the code syntax tree, making the conditional and marginal paths respect the natural nesting structure of the code. The insertion of an element would correspond to a function, or a for loop, or an entire expression enclosed by matching parentheses, etc, providing a strong inductive bias to the model via the flow trajectory.

In our current implementation, Branching Flows only duplicates elements, but we note that other strategies such as ‘duplicate and add noise’ are also viable, so long as the post-split distribution of the new elements is conditionally independent of  $Z$  given  $X_t$ . Introducing noise upon splitting might have beneficial ‘tie breaking’ effects during inference.

Also, our current models and results all assumed ordered sequences. If the elements are unordered, then Branching Flows can still be used, with adjustments. For example the model should respect the lack of ordering and be equivariant to permutations of the elements. However, even for problems that are not naturally ordered (arguably the case for QM9 small molecules, for example) initial exploration suggested that performance was much better when an order was imposed. We suspect this is due to model inadequacies when, for example, positional encoding is absent.

It is possible to solve the same problem as Branching Flows without pre-sampling the trees that couples  $X_0$  to  $X_1$ . The base process generator, split, and deletion rates that steer  $X_t$  to terminate at  $X_1$  can be directly specified, including in ways that make split and deletion rates dependent on the state  $X_t$ . We explored this

for the discrete case, using a Poisson Indel Process (Bouchard-Côté and Jordan, 2013) where it is tractable (if somewhat complicated) to sample  $X_t$  given  $X_0$  and  $X_1$  without simulation. Schemes for the continuous case, however, seemed to require full path simulation, making them somewhat less attractive to explore. We note that there are a family of schemes exploiting Theorem D.1 that use piecewise-constant but frequently resampled couplings (e.g. updated at points in time or upon split and deletion events) that can dramatically reduce the cost of full path simulation while allowing the split and deletion rates to depend on  $X_t$ .

One additional observation from this work is that, in the context of Generator Matching, the pre-sampled latent  $Z$  is likely underutilized, and Branching Flows provides a template for expanding the space of problems that can be approached in these frameworks.

Further work will explore the performance of Branching Flows in an array of different domains, and more systematically compare the benefits of different components of the process (e.g. branching-only vs deletion-only vs branching & deletion), as well as hyperparameters such as hazard distributions, and the optimal choice of base process for different kinds of problems.

## 8 Acknowledgments

This project received support from the Swedish Research Council (2024-00390 and 2023-02516) and the Knut and Alice Wallenberg Foundation (2024.0039) to B.M. Development of key dependencies (e.g. <https://github.com/MurrellGroup/Onion.jl>) used in this work was enabled by the Berzelius resource provided by the Knut and Alice Wallenberg Foundation at the National Supercomputer Centre. AI disclosure: GPT5 was used for initial drafting of some sections, which were rewritten and checked by the authors.

## References

- Albano, G. and Giorno, V. (2020). Inference on the effect of non homogeneous inputs in ornstein-uhlenbeck neuronal modeling. *Mathematical Biosciences and Engineering*, 17(1):328–348.
- Besard, T., Foket, C., and De Sutter, B. (2018). Effective extensible programming: Unleashing Julia on GPUs. *IEEE Transactions on Parallel and Distributed Systems*.
- Bezanson, J., Edelman, A., Karpinski, S., and Shah, V. B. (2017). Julia: A fresh approach to numerical computing. *SIAM Review*, 59(1):65–98.
- Billera, L., Nordlinder, H. N., and Murrell, B. (2025). Time dependent loss reweighting for flow matching and diffusion models is theoretically justified.
- Billera, L., Oresten, A., Stålmärck, A., Sato, K., Kaduk, M., and Murrell, B. (2024). The continuous language of protein structure. *bioRxiv*.
- Bouchard-Côté, A. and Jordan, M. I. (2013). Evolutionary inference via the poisson indel process. *Proceedings of the National Academy of Sciences*, 110(4):1160–1166.
- Campbell, A., Harvey, W., Weilbach, C., Bortoli, V. D., Rainforth, T., and Doucet, A. (2023). Trans-dimensional generative modeling via jump diffusion models. *ArXiv*, abs/2305.16261.
- Christ, S., Schwabeneder, D., Rackauckas, C., Borregaard, M. K., and Breloff, T. (2023). Plots.jl – a user extendable plotting api for the julia programming language.
- Danisch, S. and Krumbiegel, J. (2021). Makie.jl: Flexible high-performance data visualization for Julia. *Journal of Open Source Software*, 6(65):3349.
- Dao, T., Fu, D. Y., Ermon, S., Rudra, A., and Ré, C. (2022). Flashattention: Fast and memory-efficient exact attention with io-awareness. *ArXiv*.
- Dauparas, J., Anishchenko, I., Bennett, N., Bai, H., Ragotte, R. J., Milles, L. F., Wicky, B. I., Courbet, A., de Haas, R. J., Bethel, N., et al. (2022). Robust deep learning-based protein sequence design using proteinmpm. *Science*, 378(6615):49–56.

- Dunbar, J. and Deane, C. M. (2016). Anarci: antigen receptor numbering and receptor classification. *Bioinformatics*, 32(2):298–300.
- Felsenstein, J. (1981). Evolutionary trees from dna sequences: a maximum likelihood approach. *Journal of molecular evolution*, 17(6):368–376.
- Gat, I., Remez, T., Shaul, N., Kreuk, F., Chen, R. T. Q., Synnaeve, G., Adi, Y., and Lipman, Y. (2024). Discrete flow matching. *ArXiv*, abs/2407.15595.
- Hanke, L., Sheward, D. J., Pankow, A., Vidakovics, L. P., Karl, V., Kim, C., Urgard, E., Smith, N. L., Astorga-Wells, J., Ekström, S., et al. (2022). Multivariate mining of an alpaca immune repertoire identifies potent cross-neutralizing sars-cov-2 nanobodies. *Science advances*, 8(12):eabm0220.
- Havasi, M., Karrer, B., Gat, I., and Chen, R. T. Q. (2025). Edit flows: Flow matching with edit operations. *ArXiv*, abs/2506.09018.
- Holderrieth, P., Havasi, M., Yim, J., Shaul, N., Gat, I., Jaakkola, T., Karrer, B., Chen, R. T. Q., and Lipman, Y. (2024). Generator matching: Generative modeling with arbitrary markov processes. *ArXiv*, abs/2410.20587.
- Innes, M. (2018). Don’t unroll adjoint: Differentiating ssa-form programs. *CoRR*, abs/1810.07951.
- Innes, M., Saba, E., Fischer, K., Gandhi, D., Rudilosso, M. C., Joy, N. M., Karmali, T., Pal, A., and Shah, V. (2018). Fashionable modelling with flux. *CoRR*, abs/1811.01457.
- Jordan, K., Jin, Y., Boza, V., Jiacheng, Y., Cesista, F., Newhouse, L., and Bernstein, J. (2024). Muon: An optimizer for hidden layers in neural networks.
- Jumper, J., Evans, R., Pritzel, A., Green, T., Figurnov, M., Ronneberger, O., Tunyasuvunakool, K., Bates, R., Žídek, A., Potapenko, A., et al. (2021). Highly accurate protein structure prediction with alphafold. *nature*, 596(7873):583–589.
- Kovaltsuk, A., Leem, J., Kelm, S., Snowden, J., Deane, C. M., and Krawczyk, K. (2018). Observed antibody space: A resource for data mining next-generation sequencing of antibody repertoires. *The Journal of Immunology*, 201(8):2502–2509.
- Lipman, Y., Havasi, M., Holderrieth, P., Shaul, N., Le, M., Karrer, B., Chen, R. T. Q., Lopez-Paz, D., Ben-Hamu, H., and Gat, I. (2024). Flow matching guide and code. *ArXiv*, abs/2412.06264.
- McInnes, L., Healy, J., and Melville, J. (2020). Umap: Uniform manifold approximation and projection for dimension reduction. *ArXiv*.
- Murphy, K. and Weaver, C. (2016). *Janeway’s immunobiology*. Garland science.
- Nguyen, J., Havasi, M., Berrada, T., Zettlemoyer, L., and Chen, R. T. Q. (2025). Oneflow: Concurrent mixed-modal and interleaved generation with edit flows. *ArXiv*.
- Oresten, A., Sato, K., Stålmarch, A., Billera, L., Nordlinder, H. N., Ryder, J. C., Kaduk, M., and Murrell, B. (2025). Spontaneous emergence of symmetry in a generative model of protein structure. *bioRxiv*.
- Passaro, S., Corso, G., Wohllwend, J., Reveiz, M., Thaler, S., Somnath, V. R., Getz, N., Portnoi, T., Roy, J., Stark, H., et al. (2025). Boltz-2: Towards accurate and efficient binding affinity prediction. *BioRxiv*.
- Peebles, W. and Xie, S. (2023). Scalable diffusion models with transformers. *ArXiv*.
- Ramakrishnan, R. (2024). Qm9pack: A python package for data-mining the qm9 dataset.
- Ramakrishnan, R., Dral, P. O., Rupp, M., and Von Lilienfeld, O. A. (2014). Quantum chemistry structures and properties of 134 kilo molecules. *Scientific data*, 1(1):1–7.

- Ramon, A., Ali, M., Atkinson, M., Saturnino, A., Didi, K., Visentin, C., Ricagno, S., Xu, X., Greenig, M., and Sormanni, P. (2024). Assessing antibody and nanobody nativeness for hit selection and humanization with AbNatiV. *Nature Machine Intelligence*, 6:74–91.
- Sahoo, S. S., Arriola, M., Schiff, Y., Gokaslan, A., Marroquin, E., Chiu, J. T., Rush, A., and Kuleshov, V. (2024). Simple and effective masked diffusion language models. *ArXiv*.
- Schneuing, A., Igashov, I., Dobbelstein, A. W., Castiglione, T., Bronstein, M. M., and Correia, B. (2025). Multi-domain distribution learning for de novo drug design. *ArXiv*, abs/2508.17815.
- Shcheblyakov, D. V., Favorskaya, I. A., Dolzhikova, I. V., Korobkova, A. I., Alekseeva, I. A., Esmagambetov, I. B., Voronina, O. L., Tukhvatulin, A. I., Zubkova, O. V., Derkaev, A. A., et al. (2025). Ultra-potent rbm-specific single-domain antibody broadly neutralizes multiple sars-cov-2 variants with picomolar activity. *International Journal of Biological Macromolecules*, page 145386.
- Su, J., Lu, Y., Pan, S., Murtadha, A., Wen, B., and Liu, Y. (2023). Roformer: Enhanced transformer with rotary position embedding. *ArXiv*.
- Tong, A., Fatras, K., Malkin, N., Huguet, G., Zhang, Y., Rector-Brooks, J., Wolf, G., and Bengio, Y. (2024). Improving and generalizing flow-based generative models with minibatch optimal transport. *ArXiv*.
- Turnbull, O. M., Oglic, D., Croasdale-Wood, R., and Deane, C. M. (2024). p-iggen: a paired antibody generative language model. *Bioinformatics*, 40(11):btae659.

## A Counting and Deletion Process Flow Matching

### A.1 Counting Process CTMC

#### A.1.1 CTMC Equivalence with Counting Event Times

**Lemma A.1.** *Let  $T_1, T_2, \dots, T_n \sim H$  be independent samples from the hazard distribution  $H$ , with cumulative distribution function  $F_H(t)$  and density  $h(t)$ . Define*

$$X_t := \sum_{i=1}^n I_{\{T_i \leq t\}}.$$

*Conditioned on  $X_t = x_t$ , there are exactly  $n - x_t$  remaining jumps. Denote  $R := n - x_t$ . It holds that*

$$\mathbb{P}[X_{t+\delta} = x_t + 1 | X_t = x_t] = Rh(t)\delta + o(\delta).$$

*Proof.* Let  $T_t^+ := \min\{T_i : T_i > t\}$  denote the arrival time of the next jump at time  $t$ . Condition on the specific at risk index set  $S \subset \{1, \dots, n\}$  with  $|S| = R$ . Then for any  $i \in S$ ,

$$p_\delta := \mathbb{P}(t < T_i \leq t + \delta | T_i > t) = 1 - \frac{S(t + \delta)}{S(t)} = 1 - \frac{S(t) + \delta S'(t) + o(\delta)}{S(t)} = h(t)\delta + o(\delta),$$

noting that  $S'(t) = -h(t)S(t)$ . By independence, the number of jumps in  $(t, t + \delta]$  among the  $R$  at-risk units is Binomial( $R, p_\delta$ ), and thus

$$\mathbb{P}(X_{t+\delta} = x_t + 1 | X_t = x_t) = Rp_\delta(1 - p_\delta)^{R-1}.$$

Since  $p_\delta = h(t)\delta + o(\delta) = O(\delta)$

$$(1 - p_\delta)^{R-1} = 1 - (R - 1)p_\delta + O(p_\delta^2) = 1 + o(1),$$

it follows

$$\mathbb{P}(X_{t+\delta} = x_t + 1 | X_t = x_t) = R(h(t)\delta + o(\delta))(1 + o(1)) = Rh(t)\delta + o(\delta).$$

□

**Corollary A.2.** Fix  $z_c \in \mathbb{N}_{\geq 0}$  and define  $X_t = \sum_{i=1}^{z_c} I_{\{T_i \leq t\}}$ . Then it holds that  $X_t$  evolves as a CTMC with rate matrix

$$Q_t^{z_c}(x_t + 1|x_t) = (x_1 - x_t)h(t)I_{\{x_t < z_c\}},$$

and  $Q_t^{z_c}(x_t|x_t) = -Q_t(x_t + 1|x_t)$ , with  $Q_t^{z_c}(\cdot|x_t) = 0$  otherwise. In other words, if the event times are distributed according to  $H$ , then counting the events that have occurred up until the current time out of  $z_c$  total events corresponds to the counting flow process conditioned on  $z_c$ , starting at zero.

### A.1.2 Interarrival Times

**Theorem A.3.** Fix  $n \geq 1$ , and let  $T_1, \dots, T_n \sim H$  where  $H$  is a hazard distribution having cumulative distribution function  $F_H(t)$  and survival function  $S_H(t) = 1 - F_H(t)$ . Set

$$X_t = \sum_{i=1}^n I_{\{T_i \leq t\}}$$

and let  $T_t^+ := \min\{T_i : T_i > t\}$ . Let  $V_t = (T_t^+ | X_t = x_t)$ , and define  $W_t = V_t - t$  as the conditional inter-arrival time for the next arrival, conditioned on  $x_t$  preceding arrivals.

Denote  $R := n - x_t$  for the remaining number of events, given that  $x_t$  events already happened and that there are  $n$  events total. Then for each  $t$ , the quantile function of  $V_t$  is given by

$$F_{V_t}^{-1}(u) = F_H^{-1}(1 - S_H(t)(1 - u)^{\frac{1}{R}}),$$

where  $F_H^{-1}(y) := \inf\{y : F_H(y) \geq (y)\}$  is the quantile function for  $H$ . In particular, if  $U \sim \text{Unif}(0, 1)$ , then

$$W_t \stackrel{d}{=} F_H^{-1}\left(1 - S_H(t)(1 - U)^{\frac{1}{R}}\right) - t.$$

*Proof.* Let  $T_1, \dots, T_R \sim H$  i.i.d. denote the  $R := n - x_t$  arrival times exceeding  $t$  and fix  $t \in (0, 1)$ . For  $y \geq t$ , we have

$$G_t(y) := \mathbb{P}(T_i \leq y | T_i > t) = \frac{F_H(y) - F_H(t)}{1 - F_H(t)} = \frac{S_H(t) - S_H(y)}{S_H(t)}.$$

By independence,

$$\mathbb{P}(V_t \geq y) = \mathbb{P}(T_i \geq y | T_i > t)^R = \left(\frac{S_H(y)}{S_H(t)}\right)^R.$$

We find the quantile function  $F_{V_t}^{-1}(u) = \inf\{y : F_{V_t}(y) \geq u\}$ . It holds that

$$F_{V_t}(y) = u \iff 1 - \left(\frac{S_H(y)}{S_H(t)}\right)^R = u \iff F_H(y) = 1 - S_H(t)(1 - u)^{\frac{1}{R}},$$

which allows us to conclude

$$F_{V_t}^{-1}(u) = F_H^{-1}(1 - S_H(t)(1 - u)^{\frac{1}{R}}).$$

Let  $U \sim \text{Unif}(0, 1)$ . It is well known that passing  $U$  to the quantile function recovers the original distribution:

$$V_t \stackrel{d}{=} F_{V_t}^{-1}(U)$$

so since  $W_t = V_t - t$ , we have

$$W_t \stackrel{d}{=} F_H^{-1}\left(1 - S_H(t)(1 - U)^{\frac{1}{R}}\right) - t.$$

□

**Corollary A.4.** Fix  $z_c \geq 1$  and let  $X_t$  be a counting process with hazard distribution  $H$ . Condition on  $X_t = x_t$ , where  $x_t < z_c$ . Then there are  $z_c - x_t$  remaining events and the waiting time until the next event has distribution

$$W_t \stackrel{d}{=} F_H^{-1}\left(1 - S_H(t)(1 - U)^{\frac{1}{z_c - x_t}}\right)$$

where  $U \sim \text{Unif}(0, 1)$ . This allows us to efficiently sample the next waiting time given  $t$ ,  $x_t$  and  $z_c$ .

### A.1.3 Marginal Generator

Let  $Z_c \sim p_{Z_c}(dz_c)$  and  $Q_t^{z_c}$  specify a conditional on  $Z_c = z_c$  rate matrix of the counting flow process,

$$Q_t^{z_c}(x_t + 1|x_t) = h(t)(z_c - x_t)I_{\{x_t < z_c\}},$$

and  $Q_t^{z_c}(x_t|x_t) = -Q_t(x_t + 1|x_t)$ , with  $Q_t^{z_c}(\cdot|x_t) = 0$  otherwise — where  $h(t)$  is the hazard of a hazard distribution  $H$  supported on  $[0, 1]$ . We will recast this in terms of a time-dependent jump kernel (see Appendix D.2). This specifies a conditional process  $X_t|Z_c = z_c$ .

The time-dependent jump kernel characterizing the counting process is

$$Q_t^{z_c}(dy; x_t) = h(t)(z_c - x_t)\delta_{x_t+1}(dy),$$

corresponding to jumping from  $x_t$  to  $x_t + 1$  with rate  $h(t)(z_c - x_t)$ . Using the notion of a time-dependent linear parametrization (Billera et al., 2025), we can parametrize the infinitesimal generator corresponding to the jump process above by  $R_t^{z_c}(x) = z_c - x$ , and have a valid conditional generator matching loss be given by

$$L_{\text{cgm}}(\theta) = \mathbb{E}_{Z_c \sim p_{Z_c}, X_t \sim p_t|Z_c(dx|z_c)}[D(R_t^{Z_c}(X_t), R_t^\theta(X_t))],$$

where  $R_t^\theta(x_t)$  is emitted by the model for each realisation  $x_t$  of  $X_t$ , and  $D$  is a Bregman divergence. Note that the loss is minimized by the parameterization of the marginal generator, which coincides by linearity with the posterior averaged parameterization of the conditional generator

$$R_t(x_t) = \mathbb{E}_{Z_c \sim p_{Z_c}(dz_c|x_t)}[R_t^{Z_c}(x_t)] = \mu_{z_c|x_t} - x_t,$$

setting  $\mu_{z_c|x_t} := \mathbb{E}_{Z_c \sim p_{Z_c}(dz_c|x_t)}[Z_c]$ . The parameterization emitted by the model  $F_t^\theta(x_t)$  corresponds to a time-dependent jump kernel

$$Q_t(dy|x_t) = h(t)R_t^\theta(x_t)\delta_{x_t+1}(dy).$$

The sampling procedure corresponding to the model-emitted jump kernel is

$$X_0 \sim p_0, \quad (X_{t+\Delta t}|X_t = x_t) = \begin{cases} x_t & \text{with probability } 1 - \Delta t \cdot h(t)R_t^\theta(x_t), \\ x_t + 1 & \text{with probability } \Delta t \cdot h(t)R_t^\theta(x_t), \end{cases}$$

and when  $F_t^\theta = F_t$  we have  $X_t \sim p_t(dx)$  as  $\Delta t \rightarrow 0$ .

## A.2 Deletion Process

For the deletion process, we simply note that both the waiting time law and the marginal rates are a special case of the Counting process when the counts are either 0 (present) or 1 (deleted), and an increment is interpreted as a deletion.

As justified in Billera et al. (2025), whenever the hazard rate multiplier can be interpreted as a probability, i.e. is in the range  $[0, 1]$ , a valid conditional generator matching loss is found in the cross-entropy loss:

$$L_{\text{cgm}}(\theta) = -\mathbb{E}_{t \sim \mathcal{D}[0,1], Z \sim p_Z, X_t \sim p_t|Z(dx|z)}[\rho_t^Z(X_t) \log \rho_t^\theta(X_t) + (1 - \rho_t^Z(X_t)) \log(1 - \rho_t^\theta(X_t))]$$

where  $\rho_t^Z$  corresponds to the ground truth probability of a deletion, in this case either zero or one, and  $\rho_t^\theta$  corresponds to the predicted probability of a deletion.

## B Conditional and Marginal Paths for a Noisy Discrete Process

Here, we use an extension of Discrete Flow Matching (DFM Gat et al. (2024)) to allow time intervals  $[t_0, t_1]$ .

Let  $F_1$  and  $F_2$  be CDFs of some continuous distributions supported on  $[0, 1]$ , and let  $\omega_u \in [0, 1)$ . Then we define the schedulers:

$$\kappa_1(t) = F_1(t), \quad \kappa_2(t) = \omega_u(1 - F_1(t))F_2(t), \quad \kappa_3(t) = 1 - \kappa_1(t) - \kappa_2(t).$$

With the schedulers above, we consider the interpolant path

$$p_t(x|x_{t_0}, x_{t_1}) = \kappa_1(t)\delta_{x_{t_1}}(x) + \kappa_2(t)p_u(x) + \kappa_3(t)\delta_{x_{t_0}}(x)$$

for a uniform weighting term  $p_u$ . This choice enforces  $\ell_\kappa := \operatorname{argmin}_{j \in [m]} \frac{\dot{\kappa}_t^j}{\kappa_t^j} = 3$ . In the following, we denote  $\kappa_t^j := \kappa_j(t)$ . Define the interpolant path

$$p_t(x|x_{t_0}, x_1) := (\kappa_t^1 - \kappa_{t_0}^1 \frac{\kappa_t^3}{\kappa_{t_0}^3})\delta_{x_1}(x) + (\kappa_t^2 - \kappa_{t_0}^2 \frac{\kappa_t^3}{\kappa_{t_0}^3})p_u(x) + \frac{\kappa_t^3}{\kappa_{t_0}^3}\delta_{x_{t_0}}(x)$$

between  $x_{t_0}$  and  $x_1$  in the time-interval  $[t_0, 1]$ . This path is generated by

$$u_t(x, z|x_{t_0}, x_{t_1}) = (\dot{\kappa}_t^1 - \kappa_{t_0}^1 \frac{\dot{\kappa}_t^3}{\kappa_{t_0}^3})\delta_{x_{t_1}}(x) + (\dot{\kappa}_t^2 - \kappa_{t_0}^2 \frac{\dot{\kappa}_t^3}{\kappa_{t_0}^3})p_u(x) + \frac{\dot{\kappa}_t^3}{\kappa_{t_0}^3}\delta_z(x)$$

which follows from applying DFM Theorem 3 on the interval  $[t_0, 1]$ . In particular, let  $\alpha_1 = \kappa_t^1 - \kappa_{t_0}^1 \frac{\kappa_t^3}{\kappa_{t_0}^3}$ ,  $\alpha_2 = \kappa_t^2 - \kappa_{t_0}^2 \frac{\kappa_t^3}{\kappa_{t_0}^3}$  and  $\alpha_3 = \frac{\kappa_t^3}{\kappa_{t_0}^3}$ . It can be seen that  $\ell_\alpha := \operatorname{argmin}_{j \in [m]} \frac{\dot{\alpha}_t^j}{\alpha_t^j} = 3$ , along with  $\alpha_1, \alpha_2, \alpha_3 \geq 0$  and  $\sum_{i=1}^3 \alpha_i = 1$ . The expression for the rates thus follows from

$$\begin{aligned} \dot{\alpha}_1 - \alpha_1 \frac{\dot{\alpha}_3}{\alpha_3} &= (\dot{\kappa}_t^1 - \kappa_{t_0}^1 \frac{\dot{\kappa}_t^3}{\kappa_{t_0}^3}) - (\kappa_t^1 - \kappa_{t_0}^1 \frac{\kappa_t^3}{\kappa_{t_0}^3}) \frac{\dot{\kappa}_t^3}{\kappa_t^3} \\ &= \dot{\kappa}_t^1 - \kappa_{t_0}^1 \frac{\dot{\kappa}_t^3}{\kappa_{t_0}^3} \end{aligned}$$

and analogously

$$\dot{\alpha}_2 - \alpha_2 \frac{\dot{\alpha}_3}{\alpha_3} = \dot{\kappa}_t^2 - \kappa_{t_0}^2 \frac{\dot{\kappa}_t^3}{\kappa_{t_0}^3}.$$

## C The Ornstein-Uhlenbeck process with Time Dependent Diffusion Coefficient

Consider the stochastic differential equation

$$dX_t = \theta(\mu - X_t)dt + \sqrt{v_t}dW_t, \quad (2)$$

where  $v_t$  is the time-dependent infinitesimal variance (so the diffusion coefficient is  $\sqrt{v_t}$ ). We will, for some  $x_1$ , consider the time-inhomogeneous OU-bridge  $X_t | X_1 = x_1$  where the unconditional process  $X_t$  solves

$$dX_t = \theta(x_1 - X_t)dt + \sqrt{v_t}dW_t. \quad (3)$$

A slightly more general problem is studied in Albano and Giorno (2020), specifically of the form (See their equation (2.4))

$$dX_t = \left( -\frac{X_t}{\nu} + \mu + m_t \right) dt + \sqrt{v_t}dW_t, \quad (4)$$

where explicit formulas for the transition densities (which remain Gaussian) are given, which we use to derive bridge densities.

## D Branching Flows in Generator Matching

### D.1 Conditioning on Latent Discrete Processes

As in Edit Flows (Havasi et al., 2025) but in the more general context of Generator Matching (GM) (Holderrieth et al., 2024), we extend the theory to allow for conditioning on discrete processes. Let  $\mathcal{G}$  be discrete and let

$(X_t, G_t)$  be an  $S \times \mathcal{G}$ -valued process under the GM-regularity assumptions. Here, we suppose that for each fixed  $g \in \mathcal{G}$  there is an operator  $\mathcal{L}_t^g : \mathcal{T} \rightarrow C(S; \mathbb{R})$  generating  $p_{X_t, G_t}(dx, g)$ :

$$\partial_t \int_S f(x) p_{X_t, G_t}(dx, g) = \int_S \mathcal{L}_t^g f(x) p_{X_t, G_t}(dx, g).$$

**Theorem D.1.** *Let  $(X_t, G_t)$  be an  $S \times \mathcal{G}$ -valued stochastic process satisfying the GM-regularity assumptions, where  $\mathcal{G}$  is discrete. Then*

$$\mathcal{L}_t f(x) := \sum_{g \in \mathcal{G}} \mathcal{L}_t^g f(x) p_{G_t | X_t}(g | x)$$

generates  $p_t(dx)$ , i.e.,  $\mathcal{L}_t$  solves the KFE for  $p_t$ :

$$\partial_t \int f(x) p_t(dx) = \int \mathcal{L}_t f(x) p_t(dx).$$

Moreover, assume that  $F_t^g : S \rightarrow \Omega \subset V$  is a linear parametrization of  $\mathcal{L}_t^g f(x)$  over a fixed vector space  $V$ . If there is a linear  $\mathcal{K} : \mathcal{T} \rightarrow \mathcal{C}(S; V)$  on the inner product space  $\langle \cdot, \cdot \rangle_V$  such that

$$\mathcal{L}_t^g f(x) = \langle \mathcal{K} f(x), F_t^g(x) \rangle_V$$

for each  $g \in \mathcal{G}$ , then

$$F_t(x) = \mathbb{E}_{G_t \sim p_{G_t | X_t}(dg | x)} [F_t^{G_t}(x)]$$

linearly parametrizes  $\mathcal{L}_t$ .

*Proof.* For each  $t \in [0, 1]$ , we have  $p_t(dx) = \sum_{g \in \mathcal{G}} p_t(dx, g)$ , and hence:

$$\begin{aligned} \partial_t \int_S f(x) p_t(dx) &= \partial_t \int_S f(x) \sum_{g \in \mathcal{G}} p_t(dx, g) \\ &= \sum_{g \in \mathcal{G}} \partial_t \int_S f(x) p_t(dx, g) \\ &= \sum_{g \in \mathcal{G}} \int_S \mathcal{L}_t^g f(x) p_t(dx, g) \\ &= \sum_{g \in \mathcal{G}} \int_S \mathcal{L}_t^g f(x) p_{G_t | X_t}(g | x) p_t(dx) \\ &= \int_S \left( \underbrace{\sum_{g \in \mathcal{G}} \mathcal{L}_t^g f(x) p_{G_t | X_t}(g | x)}_{=\mathcal{L}_t f(x)} \right) p_t(dx). \end{aligned}$$

By the linearity of expectations and the map  $w \mapsto \langle v, w \rangle_V$  for fixed  $v \in V$ , we have

$$\begin{aligned} \mathcal{L}_t f(x) &= \mathbb{E}_{G_t \sim p_{G_t | X_t}(dg | x)} [\mathcal{L}_t^{G_t} f(x)] \\ &= \mathbb{E}_{G_t \sim p_{G_t | X_t}(dg | x)} [\langle \mathcal{K} f(x), F_t^{G_t}(x) \rangle_V] \\ &= \langle \mathcal{K} f(x), \mathbb{E}_{G_t \sim p_{G_t | X_t}(dg | x)} [F_t^{G_t}(x)] \rangle_V \\ &= \langle \mathcal{K} f(x), F_t(x) \rangle_V. \end{aligned}$$

□

**Theorem D.2.** *The latent-process-conditioned generator matching loss and the standard generator matching loss coincide up to a constant in  $\theta$ :*

$$\nabla_\theta \mathbb{E}_{t \sim \mathcal{D}, X_t, G_t \sim p_t(dx, dg)} D(F_t^{G_t}(X_t), F_t^\theta(X_t)) = \nabla_\theta \mathbb{E}_{t \sim \mathcal{D}, X_t \sim p_t(dx)} [D(F_t(X_t), F_t^\theta(X_t))].$$

*Proof.* Since expectations commute with the left slot of Bregman divergences under the gradient, we obtain:

$$\begin{aligned}
\nabla_{\theta} \mathbb{E}_{t \sim \mathcal{D}, X_t, G_t \sim p_t(dx, dg)} D(F_t^{G_t}(X_t), F_t^{\theta}(X_t)) &= \nabla_{\theta} \mathbb{E}_{t \sim \mathcal{D}, X_t \sim p_t(dx)} \mathbb{E}_{G_t \sim p_{G_t|X_t}(dg|x)} D(F_t^{G_t}(X_t), F_t^{\theta}(X_t)) \\
&= \mathbb{E}_{t \sim \mathcal{D}, X_t \sim p_t(dx)} \nabla_{\theta} \mathbb{E}_{G_t \sim p_{G_t|X_t}(dg|x)} D(F_t^{G_t}(X_t), F_t^{\theta}(X_t)) \\
&= \mathbb{E}_{t \sim \mathcal{D}, X_t \sim p_t(dx)} \nabla_{\theta} D(\mathbb{E}_{G_t \sim p_{G_t|X_t}(dg|x)} [F_t^{G_t}(X_t)], F_t^{\theta}(X_t)) \\
&= \mathbb{E}_{t \sim \mathcal{D}, X_t \sim p_t(dx)} \nabla_{\theta} D(F_t(X_t), F_t^{\theta}(X_t)) \\
&= \nabla_{\theta} \mathbb{E}_{t \sim \mathcal{D}, X_t \sim p_t(dx)} D(F_t(X_t), F_t^{\theta}(X_t)).
\end{aligned}$$

□

**Remark D.3.** The arguments in Holderrieth et al. (2024) allow us to include an additional latent conditioning variable  $z \in \mathcal{Z}$  that is often used to steer the path towards terminating at a particular point of the data distribution. Let  $\mathcal{L}_t^{z,g}$  denote the conditional generator given  $z \in \mathcal{Z}$  and  $g \in \mathcal{G}$ . Define the  $z$ -conditioned generator

$$\mathcal{L}_t^z f(x) := \mathbb{E}_{G_t \sim p_{G_t|X_t, z}(dg|x, z)} [\mathcal{L}_t^{z, G_t} f(x)].$$

Then, by Theorem D.1 and Proposition 1 of GM,

$$\begin{aligned}
\mathbb{E}_{Z \sim p_Z|X_t}(dz|x), G_t \sim p_{G_t|Z, X_t}(dg|z, x) [\mathcal{L}_t^{Z, G_t} f(x)] &= \mathbb{E}_{Z \sim p_Z|X_t}(dz|x) [\mathbb{E}_{G_t \sim p_{G_t|Z, X_t}(dg|z, x)} [\mathcal{L}_t^{Z, G_t} f(x)]] \\
&= \mathbb{E}_{Z \sim p_Z|X_t}(dz|x) [\mathcal{L}_t^Z f(x)] \\
&= \mathcal{L}_t f(x),
\end{aligned}$$

so averaging over a fixed  $z \in \mathcal{Z}$  and a discrete process  $(G_t)_{0 \leq t \leq 1}$  recovers the same marginal generator  $\mathcal{L}_t$ . For the loss, if we write  $F_t^{z,g}$  for a linear parametrization of  $\mathcal{L}_t^{z,g}$ , the same linearity argument as in Theorem D.2 gives

$$\begin{aligned}
\nabla_{\theta} \mathbb{E}_{t \sim \mathcal{D}, X_t, Z, G_t} D(F_t^{Z, G_t}(X_t), F_t^{\theta}(X_t)) &= \mathbb{E}_{t \sim \mathcal{D}, X_t} [\nabla_{\theta} \mathbb{E}_{Z \sim p_Z|X_t}(dz|x), G_t \sim p_{G_t|Z, X_t}(dg|z, x) [D(F_t^{Z, G_t}(X_t), F_t^{\theta}(X_t))]] \\
&= \mathbb{E}_{t \sim \mathcal{D}, X_t} [\nabla_{\theta} D(\mathbb{E}_{Z \sim p_Z|X_t}(dz|x), G_t \sim p_{G_t|Z, X_t}(dg|z, x) [F_t^{Z, G_t}(X_t)], F_t^{\theta}(X_t))] \\
&= \mathbb{E}_{t \sim \mathcal{D}, X_t} \nabla_{\theta} D(F_t(X_t), F_t^{\theta}(X_t)) \\
&= \nabla_{\theta} \mathbb{E}_{t \sim \mathcal{D}, X_t} D(F_t(X_t), F_t^{\theta}(X_t)),
\end{aligned}$$

so conditioning on a fixed  $z \in \mathcal{Z}$  does not change the gradient of the loss.

**Remark D.4.** Analogues of these theorems also hold when  $\mathcal{G}$  is an arbitrary state space (i.e., a Polish metric space endowed with its Borel  $\sigma$ -algebra), which will be considered in a forthcoming manuscript.

**Remark D.5.** Each of the preceding notions also holds for time and state dependent linear parametrizations and Bregman divergences, possibly reweighted by an integrable function  $w : [0, 1] \rightarrow \mathbb{R}_{\geq 0}$  such that  $w(t) > 0$  for Lebesgue almost every  $t \in [0, 1]$ , with the expectation in the loss taken with respect to any time distribution  $D$  dominating the Lebesgue measure, as in Billera et al. (2025).

## D.2 The Infinitesimal Generator of Jump Processes

In line with Generator Matching (GM) (Holderrieth et al., 2024) and Flow Matching Guide (FMG) (Lipman et al., 2024), we model jumps by a time-dependent kernel  $Q_t(dy; x)$  that, for each state  $x \in S$ , assigns a positive measure on  $S \setminus \{x\}$ . Its total mass

$$\lambda_t(x) = \int Q_t(dy; x)$$

gives the jump intensity or jump rate, i.e. the instantaneous hazard of leaving  $x$ , and we require  $\lambda_t(x) < \infty$ . When  $\lambda_t(x) > 0$ , normalizing  $Q_t$  yields the jump destination distribution

$$J_t(dy; x) = \frac{Q_t(dy; x)}{\lambda_t(x)},$$

which is a probability measure on  $S \setminus \{x\}$ . Now we see how specifying a jump kernel  $Q_t(dy; x)$  describes a jump process. With the hazard/rate of  $\lambda_t(x)$ , we will jump to a point  $y \sim J_t(dy; x)$ . The sampling procedure is thus as follows:

$$(X_{t+\Delta t} | X_t = x_t) = \begin{cases} X_t & \text{with probability } 1 - \Delta t \lambda_t(x_t) + o(\Delta t) \\ \sim J_t(dy; x_t) & \text{with probability } \Delta t \lambda_t(x_t) + o(\Delta t) \end{cases}.$$

The infinitesimal generator  $\mathcal{L}_t$  associated to a process with jump measure  $Q_t$  becomes

$$\mathcal{L}_t f(x) = \int (f(y) - f(x)) Q_t(dy; x)$$

As in TDLR (Billera et al., 2025) we consider atomic time-dependent jump kernels:

$$Q_t(dy; x) = \sum_{i=1}^n \lambda_i(t, x) \delta_{\Gamma_i(t, x)}(dy),$$

specifying *jump targets*  $\Gamma_i(t, x)$  and *jump rates*  $\lambda_i(t, x)$ . The total rate is

$$\lambda_{\text{total}}(t, x) := \int Q_t(dy; x) = \sum_{i=1}^n \lambda_i(t, x)$$

and the normalized jump distribution  $J_t(dy; x)$  is

$$J_t(dy; x) = \frac{1}{\lambda_{\text{total}}(t, x)} \sum_{i=1}^n \lambda_i(t, x) \delta_{\Gamma_i(t, x)}(dy),$$

so that if  $Y \sim J_t(dy|x)$ , then  $\mathbb{P}(Y = \Gamma_i(t, x)) = \frac{\lambda_i(t, x)}{\lambda_{\text{total}}(t, x)}$  for  $i = 1, \dots, n$ .

### D.3 The Branching Infinitesimal Generator

In this section, we simply denote  $\mathcal{E}$  for a general component-wise state space, augmented or not.

Let  $S := \bigsqcup_{n \geq 1} \mathcal{E}^n = \{(x, n) : x \in \mathcal{E}^n, n \geq 1\}$ . For this section and elsewhere in the paper, we often denote elements  $(x, n) \in S$  simply by  $x \in S$  for convenience. We let  $h_{\text{inc}}(t) > 0$  and  $h_{\text{del}}(t) > 0$  be overall hazard multipliers such that  $h_{\text{inc}}(t) \rightarrow \infty$  and  $h_{\text{del}}(t) \rightarrow \infty$  as  $t \nearrow 1$ , corresponding to an overall rate multiplier for split increments and an overall rate multiplier for deletions, as in Section 2.3.1 and Section 2.3.2. Suppose that splitting of the  $i$ 'th component out of  $n$ -components occurs with rate  $R_{t,i}(x, n) h_{\text{inc}}(t)$  and that deletion of the  $i$ 'th component out of  $n$ -components occurs with rate  $\rho_{t,i}(x, n) h_{\text{del}}(t)$ . Here,  $R_{t,i}(x, n) \geq 0$  is intended to indicate the 'remaining number of splits of the  $i$ 'th component' and  $\rho_{t,i}(x, n) \in [0, 1]$  is intended to indicate the 'probability of deleting the  $i$ 'th component'.

In this section, we arrive at a time- and state varying linear parametrization for the infinitesimal generator of our branching process. The notion of a linear parametrization of a generator, introduced in GM and further discussed in FMG, was clarified to be able to vary with both time and state in TDLR.

In what follows, for the sake of brevity we write  $f(x) := f(x, n)$ ,  $R_t(x) := R_t(x, n)$ , etc., whenever  $(x, n) \in S$ . We find a time- and state varying linear parametrization of the branching generator of the form

$$\mathcal{L}_t^{\text{branch}} f(x, n) = \langle \mathcal{K}_{t,n}^{\text{split}} f(x), R_t(x) \rangle_{t,n}^{\text{split}} + \langle \mathcal{K}_{t,n}^{\text{del}} f(x), \rho_t(x) \rangle_{t,n}^{\text{del}} + \langle \mathcal{K}_{t,n}^{\text{base}} f(x), F_t^{\text{base}}(x) \rangle_{t,x}^{\text{base}}.$$

Using an atomic time-dependent jump kernel as in TDLR, splits and deletions as above correspond to

$$Q_t(dy; (x, n)) = \sum_{i=1}^n h_{\text{inc}}(t) R_{t,i}(x) \delta_{\text{split}_i(x)}(dy) + \sum_{i=1}^n h_{\text{del}}(t) \rho_{t,i}(x) \delta_{\text{del}_i(x)}(dy).$$

For each  $f \in \mathcal{T}(S)$ , viewing  $f(x, n) = f(x)$  where it is convenient, the infinitesimal generator for jumps becomes

$$\begin{aligned}\mathcal{L}_t^{\text{jump}} f(x, n) &= \int_S (f(y) - f(x)) Q_t(dy; (x, n)) \\ &= \int_S \left( (f(y) - f(x)) [h_{\text{inc}}(t) \cdot \sum_{i=1}^n R_{t,i}(x) \delta_{\text{split}_i(x)}(dy) + h_{\text{del}}(t) \cdot \sum_{i=1}^n \rho_{t,i}(x) \delta_{\text{del}_i(x)}(dy)] \right) \\ &= h_{\text{inc}}(t) \cdot \sum_{i=1}^n \left( (f(\text{split}_i(x)) - f(x)) R_{t,i}(x) \right) + h_{\text{del}}(t) \cdot \sum_{i=1}^n \left( (f(\text{del}_i(x)) - f(x)) \rho_{t,i}(x) \right).\end{aligned}$$

We express the jump generator in terms of a time-and-state varying linear parametrization of the generator, as is justified in TDLR, one for splitting and one for deletion. For  $v, w \in \mathbb{R}^n$ , we define the time-varying inner products

$$\langle v, w \rangle_{t,n}^{\text{split}} := h_{\text{inc}}(t) \langle v, w \rangle_{\mathbb{R}^n} \quad \text{and} \quad \langle v, w \rangle_{t,n}^{\text{del}} := h_{\text{del}}(t) \langle v, w \rangle_{\mathbb{R}^n}.$$

Note that those are inner products, since  $h_{\text{inc}}(t) > 0$  and  $h_{\text{del}}(t) > 0$ . This allows us to express

$$\mathcal{L}_t^{\text{jump}} f(x, n) = \langle \mathcal{K}_{t,n}^{\text{split}} f(x), R_t(x) \rangle_{t,n}^{\text{split}} + \langle \mathcal{K}_{t,n}^{\text{del}} f(x), \rho_t(x) \rangle_{t,n}^{\text{del}}.$$

In the above, we set:

$$\mathcal{K}_{t,n}^{\text{split}} f(x) = (f(\text{split}_i(x)) - f(x))_{i=1}^n$$

and

$$\mathcal{K}_{t,n}^{\text{del}} f(x) = (f(\text{del}_i(x)) - f(x))_{i=1}^n.$$

In between jumps, we assume that the process evolves according to a base generator on each branch level — this could, for example, correspond to an SDE. We assume that we have a linear parametrization

$$\mathcal{L}_t^{\text{base}} f(x, n) = \langle \mathcal{K}_{t,n}^{\text{base}} f(x), F_t^{\text{base}}(x) \rangle_{t,x}^{\text{base}}$$

for the base process along each branch. This results in

$$\begin{aligned}\mathcal{L}_t^{\text{branch}} f(x, n) &= \mathcal{L}_t^{\text{jump}} f(x, n) + \mathcal{L}_t^{\text{base}} f(x, n) \\ &= \langle \mathcal{K}_{t,n}^{\text{split}} f(x), R_t(x) \rangle_{t,n}^{\text{split}} + \langle \mathcal{K}_{t,n}^{\text{del}} f(x), \rho_t(x) \rangle_{t,n}^{\text{del}} + \langle \mathcal{K}_{t,n}^{\text{base}} f(x), F_t^{\text{base}}(x) \rangle_{t,x}^{\text{base}}.\end{aligned}$$

## D.4 The Branching Flows Loss

The conditional branching flows loss is the conditional generator matching loss associated to the linear parametrization from Appendix D.3. We specify a conditional infinitesimal generator of the form

$$\mathcal{L}_t^{z,g,\text{branch}} f(x, n) = \langle \mathcal{K}_{t,n}^{\text{split}} f(x), R_t^{z,g}(x) \rangle_{t,n}^{\text{split}} + \langle \mathcal{K}_{t,n}^{\text{del}} f(x), \rho_t^{z,g}(x) \rangle_{t,n}^{\text{del}} + \langle \mathcal{K}_{t,n}^{\text{base}} f(x), F_t^{z,g,\text{base}}(x) \rangle_{t,x}^{\text{base}}.$$

and we similarly specify a model parametrized infinitesimal generator

$$\mathcal{L}_t^{\theta,\text{branch}} f(x, n) = \langle \mathcal{K}_{t,n}^{\text{split}} f(x), R_t^\theta(x) \rangle_{t,n}^{\text{split}} + \langle \mathcal{K}_{t,n}^{\text{del}} f(x), \rho_t^\theta(x) \rangle_{t,n}^{\text{del}} + \langle \mathcal{K}_{t,n}^{\text{base}} f(x), F_t^{\theta,\text{base}}(x) \rangle_{t,x}^{\text{base}}.$$

As in TDLR, when a generator is expressed as a sum of linear parametrizations, a valid per-term conditional generator matching loss is then the sum of Bregman divergences

$$D_{t,x}^{\text{split}}(R_t^{z,g}(x), R_t^\theta(x)) + D_{t,x}^{\text{del}}(\rho_t^{z,g}(x), \rho_t^\theta(x)) + D_{t,x}^{\text{base}}(F_t^{z,g,\text{base}}(x), F_t^{\theta,\text{base}}(x)),$$

again noting that  $x$  stands for  $(x, n) \in S$ . Assuming that  $R_t^{z,g}(x)$  can be interpreted as the remaining number of splits for each component and that  $\rho_t^{z,g}(x)$  can be interpreted as deletion probabilities, we choose a Poisson-like Bregman for splits and a cross-entropy loss for deletions.

Note that these loss functions require a notion of Bregman divergence associated with convex functions that are only differentiable on a subset of their domain, as considered in TDLR.

If we also assume that the base Bregman divergence is separable and splits along each component, the conditional branching flows loss becomes:

$$\begin{aligned}
 L_{\text{CBF}}(\theta) = & \mathbb{E}_{t \sim \mathcal{D}[0,1], Z \sim p_Z, (X_t, G_t) \sim p_{X_t, G_t|Z}(dx, dg|z)} \\
 & \left[ \sum_{i=1}^{N_{X_t}} \left( R_{t,i}^\theta(X_t) - R_{t,i}^{Z, G_t}(X_t) \log R_{t,i}^\theta(X_t) \right) \right. \\
 & + \sum_{i=1}^{N_{X_t}} \left( -[\rho_{t,i}^{Z, G_t}(X_t) \log \rho_{t,i}^\theta(X_t) + (1 - \rho_{t,i}^{Z, G_t}(X_t)) \log(1 - \rho_{t,i}^\theta(X_t))] \right) \\
 & \left. + \sum_{i=1}^{N_{X_t}} \left( D_{t, X_t, i}^{\text{base}}(F_{t,i}^{Z, G_t, \text{base}}(X_t), F_{t,i}^{\theta, \text{base}}(X_t)) \right) \right].
 \end{aligned}$$

## E Further Empirical Details

### E.1 QM9 analysis

10k samples from the Branching Flows QM9 model were generated with a step schedule  $t = 1 - (\cos(\pi s) + 1)/2$  for  $s \in (0, 1/1000, 2/1000, \dots, 1)$ .

We study the QM9 Branching Flows model outputs by comparison to the QM9 data, comparing marginal distributions of atom counts (total, carbon, nitrogen, oxygen, fluorine, and hydrogen), and molecular properties. Atom counts are read directly from the .xyz model output or QM9 data.

For molecule properties, since the training samples and model-generated samples are atom point clouds (ie. no bond structure is explicitly represented), we use OpenBabel to convert .xyz coordinates to .sdf, which also infers bond structure and SMILES strings. The .sdf is then read into RDKit for downstream analysis, and computing molecule properties, and fingerprints. OpenBabel was run using the OpenBabel.jl Julia wrapper, and RDKit was run using the MoleculeFlow.jl Julia wrapper.

We discard any molecules that are invalid, where invalid includes molecules that RDKit returns a ‘valid=false’ flag, or where the molecule is not fully connected. Importantly, not all true QM9 molecules can be successfully parsed by RDKit from the .xyz files, and we apply identical filtering to both true and generated sets. After .xyz  $\rightarrow$  .sdf conversion, 9882 of 10k QM9 molecules are ‘valid=true’ by RDKit and, of these, none were not fully connected. For Branching Flows generated molecules, 9871 of 10k are ‘valid=true’ and, of these, 58 were not fully connected. Thus 9882 for QM9 data and 9813 for Branching Flows generated molecules were used to compare distributions.

Molecular fingerprints encode the structural features of a molecule into a fixed-length bit vector which can be used for similarity search, clustering, etc. Here, we compute the ‘RDKit fingerprints’ (using MoleculeFlow.jl) and embed these in two dimensions, using Uniform Manifold Approximation (run via UMAP.jl, with default settings). This is used to visualize the distribution of true QM9 and generated samples.

We used the model from Campbell et al. (2023) to generate 10,000 samples, and analyze them as above. Note: the UMAPs, which are computed jointly from all the samples, will differ in the analysis that includes transdimensional jump samples.

To quantify univariate distribution overlap, we use a Kolmogorov-Smirnov-like statistic between the empirical cumulative distribution functions of samples  $Y$  from each model against QM9 data. We use  $1 - KS_D$ , where

$$KS_D = \max_x |\hat{F}_Y(x) - \hat{F}_{QM9}(x)|$$

where  $\hat{F}$  denotes the empirical CDF. This statistic is 1 when the distributions agree perfectly, and 0 when they do not overlap at all.

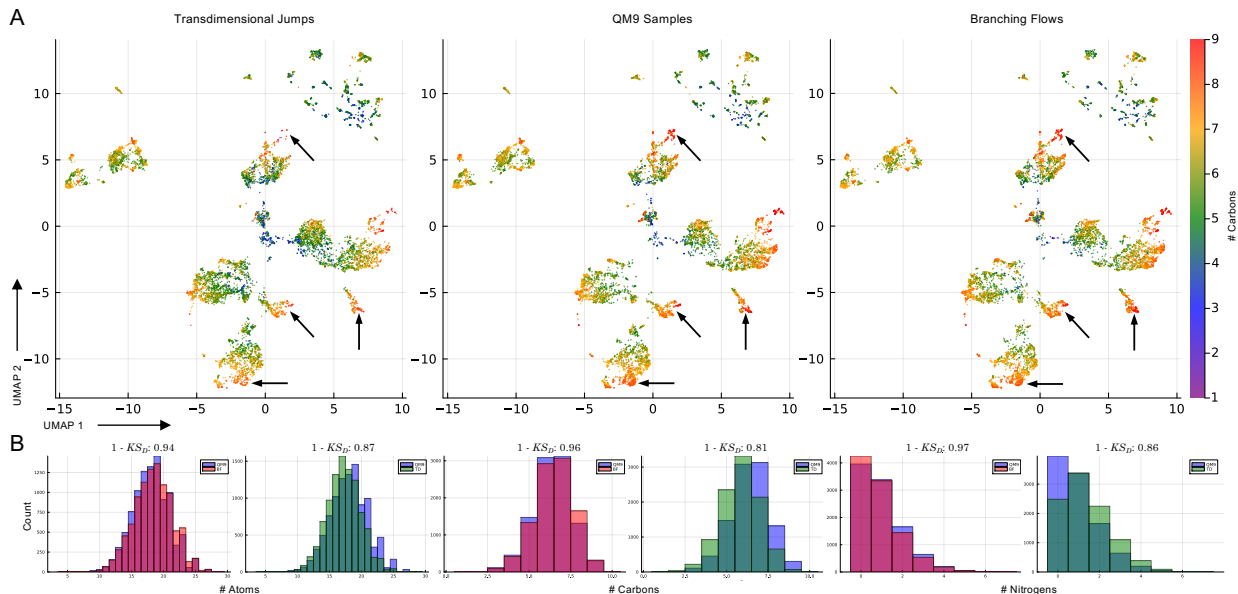


Figure 10: **Transdimensional Jump Diffusion and Branching Flows.** **A.** UMAP embeddings from molecular fingerprints for samples from a Transdimensional Jump Diffusion model (Campbell et al., 2023), from QM9 data, and from Branching Flows. Matched black arrows show regions where the data distribution has a high density of molecules with 8 or 9 carbons, which appears to be undersampled with Transdimensional Jumps. **B.** Histograms showing the distributions for Branching Flows (BF) vs QM9 and Transdimensional Jumps (TD) vs QM9, selected from the more extreme differences in Table 1.

## E.2 Antibodies

### E.2.1 Antibody Sequence Generation: Metrics and Comparisons

To evaluate Branching Flows, 10 000 sequences were generated with 1 000 uniformly-spaced steps from Branching Flows, Oracle Length, and Edit Flows models and then compared to natural ones. Sequence diversity was assessed by computing the minimum pairwise cosine distance (over vectors of 3-mer counts) within each set. Sequence ‘novelty’ was evaluated by computing the minimum Levenshtein distance to any sequence in a hold-out validation data set (needed because otherwise the novelty of all natural sequences would be zero).

Sequence ‘nativeness’ was computed using AbNatiV Ramon et al. (2024). Finally, the distribution of amino acids, distribution of sequence lengths and the distribution of CDR3 lengths were also computed. The latter was computed using ANARCI Dunbar and Deane (2016).

For investigating the training dynamics of Branching Flows compared to Oracle Length and Edit Flows models the losses cannot be directly compared, so after every 500 steps during training, 5 sequences were generated (with 200 uniformly-spaced steps) and saved. The perplexity of the generated sequences was computed as evaluated by a 130 million parameter autoregressive model trained on the data from Turnbull et al. (2024).

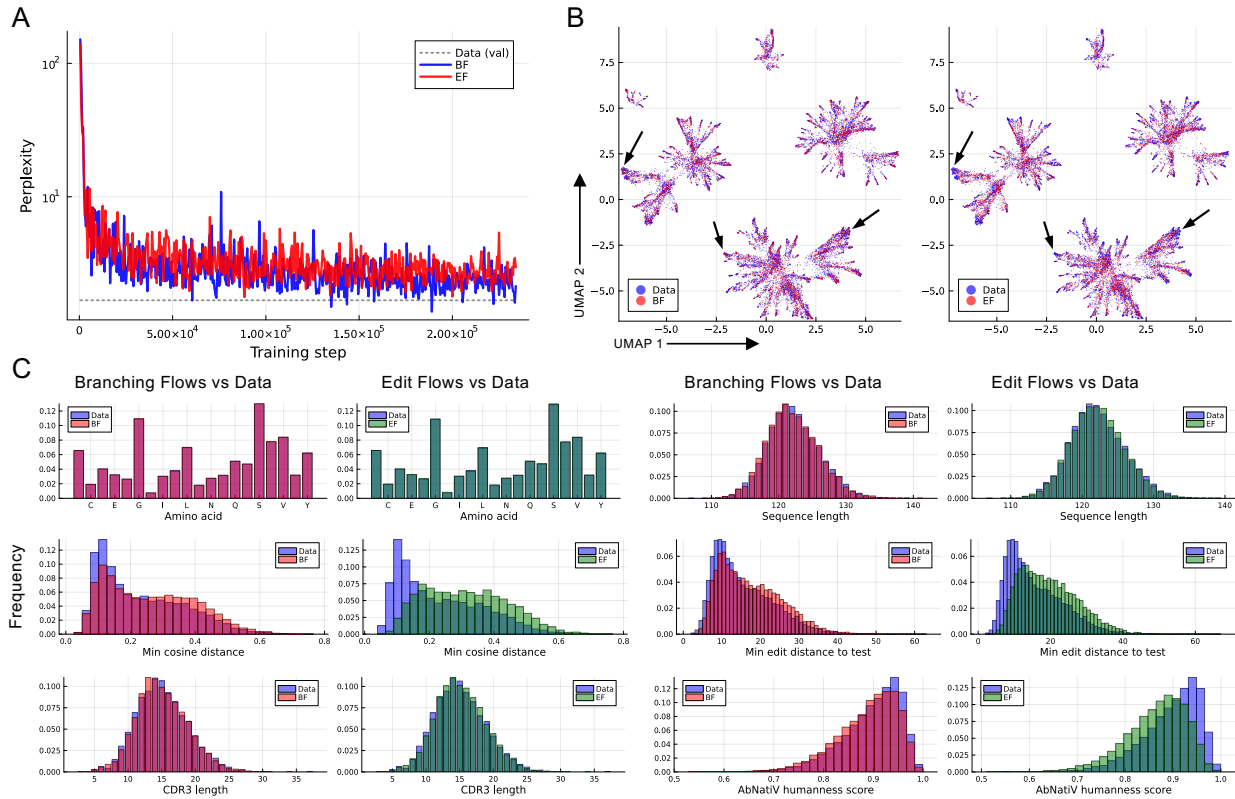


Figure 11: **Branching Flows vs Edit Flows.** **A** The perplexity, evaluated under an autoregressive LLM, of samples generated by Branching Flows (BF) vs Edit Flows (EF), which is a discrete-only variable length flow matching strategy. This is shown over training iterations. **B** two seqUMAP (Hanke et al., 2022) plots comparing Branching Flows and Edit Flows (respectively) each against real sequences. Arrows point to regions, at the extremities of the UMAP-embedded shapes, where Edit Flows density appears to be reduced. **C** Comparison of several distributions of the generated sequences with sequences from the validation data set.